博士学位請求論文

論文題目　　　Development of Novel Functional Inhibitor for Mitotic Kinesin Eg5 as a target cancer Therapy

専　攻　名　　　工学研究科生命情報工学専攻

学籍番号　　　19d5602

氏　　　名　　　Islam Md Alrazi

指導教員　　　丸田　晋策

創 価 大 学 大 学 院
工 学 研 究 科

Development of novel functional inhibitor for mitotic kinesin Eg5 as a target cancer therapy

「がん治療の標的である有糸分裂キネシン **Eg5** の新規機能性 阻害剤の開発」

2022

ISLAM MD ALRAZI

Dedicated to

My dearest, respected parents and my teachers

Acknowledgments

Abstract

Kinesin is a motor protein that plays an important role in animal and plant cells. It hydrolyzes ATP and moves along microtubules. It means that motor proteins are extremely fine machines that can efficiently convert the chemical energy produced by ATP hydrolysis into mechanical energy. In fact, martin et.al. (2007) propose that motor proteins could be applied to various fields as '' nanomachines''. Eg5 belongs to the motor protein. It involves in the transport of the endoplasmic reticulum and organelles, and the transport of neurotransmitters from nerve bodies to synaptic terminals in nerve axons. It also plays a crucial role in mitotic cell division for the formation of the bipolar spindle in the eukaryotic cell division. Therefore, it has been suggested that mitotic kinesin Eg5 is considered a potential target for cancer therapy.

The various functions of Eg5 are proposed in equivalent polymorphisms in the key kinesin structural elements. One of the functional elements of Eg5 is referred to as Loop 5(L5). Especially, L5 of Eg5 has a very long structure unlike other kinesins and acts as the target for binding of small molecular inhibitors. For the application of Eg5 motor proteins as nanomachines, it is essential to artificially control the mechanical structure that changes with external stimulation. Some of the results have continued for the development of inhibitors for Eg5. Interestingly, several small-molecule compounds (such as monastrol, S-Triyl-L-Cysteine (STLC), Ispinesib, and so on) have been shown the Eg5 inhibitory activity. They are binding to the same druggable Eg5 allosteric pocket, which is composed of Loop L5, $\alpha2$, and $\alpha3$. However, they showed structural diversity and control the activity of Eg5 unidirectionally or irreversibly. They could not be applied as nanodevice to control the functional activity of Eg5 reversibly. Therefore, switching is required to control Eg5 activity reversibly not only in general but also in functional.

To do that, I focused on chromism. Chromism refers to a phenomenon in which the optical properties (color, fluorescence, etc.) of a substance are reversibly changed by external stimulation such as heat, pH, light, and so on. A substance that exhibits chromism is called a chromic substance (or chromic material). First, it is suggested that heat could work as a switching like as- high, low, and room temperature. However, in this study, I have used a protein that is highly sensitive to high temperatures. Therefore, thermal is not an appropriate technique for switching. Subsequently, I focused on the development of switching with different pH like as- acidic, alkaline, and neutral pH. Unfortunately, both the acidic and alkaline pH is harmful to the general structure of the protein. Hence, pH could not be applicable for working as a switching. Finally, I focused on light for the establishment of switching. It has been well known that photochromic compounds show light sensitivity. Photochromic compounds are those compounds that show their structural and functional changes depends upon the light irritation. There are two types of mechanisms observed for returning to their original states. A mechanism that returns by irradiating light with a different wavelength, it's called P-type such as diarylethene and fulgide. Another one, a mechanism that returns by heat, it's called T-type such as spiropyran, azobenzene, and stilbenes.

Interestingly, some of the photochromic compounds showed structural similarity with well-known potent Eg5 inhibitors such as spiropyran. Sadakane, et.al, designed and synthesized a novel photochromic Eg5 inhibitor composed of double photochromic compounds, spiropyran, and azobenzene. The inhibitor displayed two isomerization states and controlled Eg5 activity. Generally, one photochromic compound shows two isomerization states. Theoretically, coupling of two different photochromic compounds could show multiple isomerization states which would be effective to establish photo switching precisely. In our laboratory, photo switching has been using as a well-established technique to control protein activity for the last two decades. I focused on obtaining novel inhibitors from synthetic or

natural sources and then react with photochromic compounds. The most changeling task is designing of photochromic inhibitor for controlling Eg5 activity in multiple stages. In this study, I demonstrated to develop a novel Eg5 inhibitor which has two parts, such as- one is regulatory part, and another is inhibitory part to control Eg5 function in multiple states like strongly, weakly and mediumly.

Firstly, to achieve that, I designed and combined two different photochromic compounds such as spiropyran and azobenzene to make regulatory part and it displayed inhibitory effect in multiple states. Interestingly, merely the regulatory part exhibited control action on Eg5. Secondly, I focused on to discover a new and potent Eg5 inhibitor from natural sources for the inhibitory part. Eg5 inhibitor from natural sources that I utilized in this research is Kolaroflavon and which exhibited effective control action for Eg5. In the future, that could be formed multiple states with photochromic compounds (e.g- STLC- Azobenzene derivatives, Ishikawa et.al). The aim of the study, the formation of multiple states have the clinical significance for the treatment of cancer patients. The inhibitory activity of drugs could be controlled precisely, in terms of high dosage, low dosage, or medium dosage, considering the patient's condition.

Key words: Kinesin, Kinesin Eg5, Mitosis cell division, Loop 5, Eg5 inhibitors, Photochromic compound, Isomerization.

Abbreviations

ATP	Adenosine-5'-triphosphate
ADP	Adenosine-5'-diphosphate
Da	Dalton
DTT	Dithiothreitol
DMF	N,N- dimethylformamide
THF	Tetrahydrofuran
PIPES	Piperazine-1,4-bis (2-ethanesulfonic acid)
EGTA	O,O'- Bis (2-aminoethyl)ethylene-N,N,N',N'- tetra acetic acid
EDTA	Ethylenediamine-N,N,N',N'-tetra acetic acid
TCA	Trichroloacetic acid
TLC	Thin-layer Chromatography
Tris	2-Amino-2-(hydroxymethyl) propane-1,3-diol
HEPES	2-4-(2-hydroxyethyl) piperazin-1-yl] ethanesulfonic acid
HOAT	1-Hydroxy-7-azabenzotriazole
EDC	1-Ethyl-3-(3-dimethylaminopropyl)carbodiimide
Pi	Phosphate

UV   Ultraviolet

VIS   Visible

MT   Microtubule

STLC   S-trityl-L-cysteine

GB   Garcinia biflavonoid

KLF   kolaflavanone

IC_{50} half maximal inhibitory concentration

SDS-PAGE   Sodium dodecyl sulphate-polyacrylamide gel electrophoresis

GTP   Guanosine-5'-triphosphate

PDB   Protein Data bank

TIP3P   Transferable intramolecular potential three-point

SD   Standard deviation

VMD   Visual molecular dynamics

LINCS   Linear Constraint Solver

MDS   Molecular dynamics simulations

Eg5   mitotic kinesin Eg5

GROMACS   Groningen Machine for Chemical Simulations

RMSD   Root Mean Square Deviation

CONTENTS

Chapter 1

General introduction

Chapter 2

Novel photochromic inhibitor for mitotic kinesin Eg5 which forms multiple isomerization states

Chapter 3

Kolaflavanone , a biflavonoid derived from medicinal plant Garcinia, is an inhibitor of mitotic kinesin Eg5

Results and Discussion

Chapter 4

List of figures

List of tables

General introduction

Motor Proteins

Motor proteins are a series of atomic engines that could move across a cell's cytoplasm. The chemical energy converted into mechanical function with the help of ATP hydrolysis. Motor proteins are responsible for a variety of functions in biological systems, including directing filament sliding during muscle contraction and facilitating intracellular trafficking along biopolymer filament tracks. As a result, motor proteins are divided into two groups based on their substrates. Actin motor protein, such as myosin, passes alongside microfilaments through contact with actin. The microtubule motor proteins are made up of dynein and kinesin and they interact with tubulins to drive microtubules. Kinesin and dynein are plus and minus-direction motors, upon the direction in which they "move" on microtubule cables inside the cell (Fig.1), (*1*).
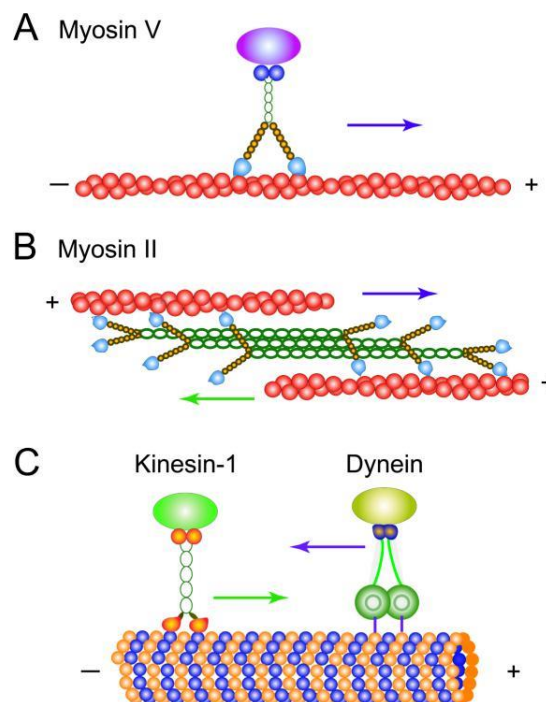
Fig. 1: Motor protein's function and their categories (Kolomeisky, Anatoly B. "Motor proteins and molecular motors: how to operate machines at the nanoscale." *Journal of Physics: Condensed Matter* 25.46 (2013): 463101.)

Motor Protein's Function

The muscle protein myosin is the well-known example of a motor protein, which induces to contraction of muscle fibers in animals. Motor proteins are responsible for most of the protein or macromolecule transport such as vehicle transport in the protoplasm. Kinesin and cytoplasmic dynein are involved in chromosomal segregation during bipolar cell division (mitosis), meiosis, the formation of spindle machinery, and intracellular transport.

Kinesin and their superfamily

Vale.et.al first discovered kinesin in neural tissue, in where it emerges to produce end-coordinated developments essential for axonal transport in addition to end-coordinated developments (2). Kinesins are classified into three types based on where the motor domain is located: N-terminal kinesins (e.g. Eg5), C-terminal kinesins (e.g. HSET) (Fig.2), and internal motor domain kinesins (3). Kinesins, alike cytoskeletal motors, have a catalytic motor domain (head) with two binding domains, one for ATP and other for microtubules. In kinesins, the neck linker connects two globular motor domains to the coiled-coil stalk (neck). A tail section at the opposite end of the stalk interacts with specific cargos and connector proteins.

To date, over 650 members of the Kinesins superfamily have been identified. They exist in all eukaryotes, whereas absent in all prokaryotes. There are over 45 different kinesins in the human genome, according to the specified motor domain and their amino acid sequence, and some of them have been associated with various diseases. Kinesins are classified into 14 subfamilies based on phylogenetic analysis of motor protein sequences, ranging from Kinesin -1 to Kinesin -14 (Table 1). The non-exclusive role in eukaryotic cells is important for cell division at various stages, organelle transport and intracellular vesicle as one of the major functions.
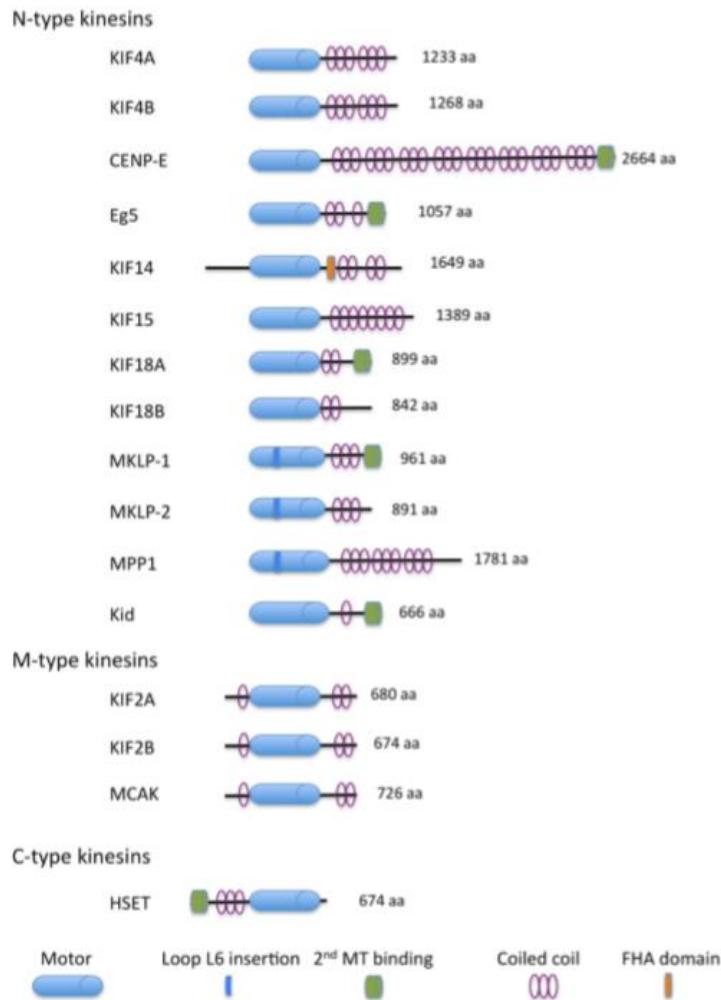
Fig.2. Human mitotic kinesins and their motors are classified. (Rath, O., & Kozielski, F. (2012). Kinesins and cancer. *Nature reviews cancer*, *12*(8), 527-539.)

Currently, 16 kinesins work together to coordinate cytokinesis and mitosis. Certainly, kinesin has been associated with the genesis, progression, and resistance of tumors in treatment development. Human kinesins have been found to be implicated in cancer and contribute to carcinogenesis. As a result, kinesins have emerged as a potential cancer treatment. Mitotic kinesin inhibitors will target Eg5, also known as KIF11, and centromere-associated protein E, and will be the most advanced with clinical features (CENPE).

Table 1. Human kinesin nomenclature and function (Rath and Kozielski, 2012)

Acronym	Full Name	Alternative Nomenclature	Kinesin Family	Function
KIF1A	kinesin family member 1A	ATSV (axonal transport of synaptic vesicles), C2orf20 (chromosome 2 open reading frame 20), FLJ30229	Kinesin-3	Neuron-specific axonal transporter of synaptic vesicle precursors
KIF1B	kinesin family member 1B	CMT2, CMT2A, HMSNII, KIAA0591, KLP, NBLST1	Kinesin-3	Microtubule plus end-directed monomeric motor protein for transport of mitochondria, involved in axonal transport
KIF1C	kinesin family member 1C	KIAA0706, LTXS1	Kinesin-3	Regulates podosome dynamics in macrophages
KIF2A	kinesin family member 2A	KIF2 (kinesin heavy chain member 2), KNS2, HK2, HsKin2	Kinesin-13	Microtubule minus end-depolymerizing motor crucial for bipolar spindle formation
KIF2B	kinesin family member 2B	FLJ53902	Kinesin-13	Involved in kinetochore-microtubule dynamics to promote mitotic progression
MCAK (KIF2C)	kinesin family member 2C	KNSL6 (kinesin-like 6), MCAK (mitotic centromere-associated kinesin)	Kinesin-13	Microtubule plus end-depolymerizing motor required for chromosome congression and alignment
KIF3A	kinesin family member 3A		Kinesin-2	Microtubule plus end-directed motor for membrane organelle

				transport, required for assembly of the primary cilium
KIF3B	kinesin family member 3B	KIAA0359	Kinesin-2	Microtubule plus end-directed motor for membrane organelle transport
KIF3C	kinesin family member 3C		Kinesin-2	Maybe involved in maturation of neuronal cells
KIF4A	kinesin family member 4A	chromokinesin-A, FLJ12530,FLJ12655, FLJ14204,FLJ20631, HSA271784, KIF4, KIF4-G1	Kinesin-4	Chromosome condensation, anaphase spindle midzone formation and cytokinesis
KIF4B	kinesin family member 4B	chromokinesin-B	Kinesin-4	Chromosome condensation, anaphase spindle midzone formation and cytokinesis
KIF5A	kinesin family member 5A	SPG10 (spastic paraplegia 10), D12S1889, MY050, NKHC	Kinesin-1	Involved in spastic paraplegia type 10 and Charcot-Marie-Tooth type 2
KIF5B	kinesin family member 5B	KNS1, KNS, UKHC	Kinesin-1	Involved in vesicle transport; interacts with a variety of viruses to allow for their replication within the cell
KIF5C	kinesin family member 5C	NKHC2, KINN, KIAA0531, FLJ44735	Kinesin-1	Binding partner of casein kinase 2 involved in apical trafficking

KIF6	kinesin family member 6	C6orf102 (chromosome 6 open reading frame 102), dJ137F1.4, dJ188D3.1, dJ1043E3.1, DKFZp451I2418, MGC33317	Kinesin-9	Unknown
KIF7	kinesin family member 7	JBTS12	Kinesin-4	Hedgehog signaling
KIF9	kinesin family member 9	MGC104186	Kinesin-9	Regulation of matrix degradation by macrophage podosomes
CENPE (KIF10)	Centromere-associated protein E	KIF10, PPP1R61 (protein phosphatase 1, regulatory subunit 61)	Kinesin-7	Microtubule-kinetochore capture and mitotic checkpoint signaling
EG5 (KIF11)	kinesin family member 11	KNSL1 (kinesin-like 1), KIF11, HKSP (Kinesin Spindle Protein), TRIP5, Thyroid receptor-interacting protein 5	Kinesin-5	Separation of the duplicated centrosome during spindle formation
KIF12	kinesin family member 12	RP11-56P10.3	Kinesin-12	Unknown
KIF13A	kinesin family member 13A	RBKIN, bA500C11.2, FLJ27232	Kinesin-3	Transports mannose-6-phosphate receptor to the plasma membrane
KIF13B	kinesin family member 13B	GAKIN, KIAA0639	Kinesin-3	Involved in regulation of neuronal cell polarity

KIF14	kinesin family member 14	CMKRP, KIAA0042, MGC142302	Kinesin-3	Involved in cytokinesis, chromosome congression and alignment
KIF15	kinesin family member 15	KNSL7 (kinesin-like 7), HKLP2, KLP2, NY-BR-62, FLJ25667	Kinesin-12	Involved in bipolar spindle formation in absence of Eg5
KIF16B	kinesin family member 16B	C20orf23 (chromosome 20 open reading frame 23), FLJ20135, dJ971B4.1, SNX23	Kinesin-3	Critical for early embryonic development by transporting the FGF receptor
KIF17	kinesin family member 17	KIAA1405, KIF3X, KIF17B	Kinesin-2	Neuron-specific molecular motor in neuronal dendrites
KIF18A	kinesin family member 18A	DKFZP434G2226, Kip3p, Klp67A, KipB, klp5/6+	Kinesin-8	Chromosome congression
KIF19	kinesin family member 19	FLJ37300, KIF19A	Kinesin-8	Unknown
MKLP-2 (KIF20A)	kinesin family member 20A	RAB6KIFL (RAB6-interacting, kinesin-like 6), MKLP-2, RabK6, rabkinesin-6, rabkinesin6, FLJ21151	Kinesin-6	Cytokinesis
MPP1 (KIF20B)	kinesin family member 20B	MPHOSPH1 (M-phase phosphoprotein 1), MPP1, CT90, KRMP1	Kinesin-6	Likely required for completion of cytokinesis
KIF21A	kinesin family	FEOM1 (fibrosis of the extraocular	Kinesin-4	Unknown

		member 21A	muscles 1), FLJ20052, KIAA1708, FEOM3A, NYREN-62		
KIF21B	kinesin family member 21B	DKFZP434J212, KIAA0449, FLJ16314	Kinesin-4	Unknown
Kid (KIF22)	kinesin family member 22	KNSL4 (kinesin-like 4), Kid (kinesin-like DNA-binding protein), OBP-1, OBP-2	Kinesin-10	Generates polar injection forces essential for chromosome congression and alignment
MKLP-1 (KIF23)	kinesin family member 23	KNSL5 (kinesin-like 5), MKLP-1 (mitotic kinesin-Like Protein 1), MKLP1, CHO1	Kinesin-6	Cytokinesis
KIF24	kinesin family member 24	C9orf48 (chromosome 9 open reading frame 48), bA571F15.4, FLJ10933, FLJ43884	Kinesin-13	Regulates centriolar length and ciliogenesis
KIF25	kinesin family member 25	KNSL3 (kinesin like 3)	Kinesin-14	Unknown
KIF26A	kinesin family member 26A	DKFZP434N178, KIAA1236, FLJ22753	Kinesin-11	Regulates GDNF-Ret signaling in enteric neuronal development
KIF26B	kinesin family member 26B	FLJ10157	Kinesin-11	Regulates adhesion of the embryonic kidney mesenchyme

KIF27	kinesin family member 27	DKFZp434D0917, RP11-575L7.3	Kinesin-4	Hedgehog signaling
HSET (KIFC1)	kinesin family member C1	KNSL2 (kinesin-like 2), HSET, Human Spleen Embryo Testes, XCTK2, Kar3, Ncd	Kinesin-14	Essential for bipolar spindle assembly and proper cytokinesis
KIFC2	kinesin family member C2		Kinesin-14	Transports vesicles in a microtubule-dependent manner in a retrograde direction62,63KIFC3kinesin
KIFC3	kinesin family member C3	FLJ34694, DKFZp686D23201	Kinesin-14	Cooperates with cytoplasmic dynein in Golgi positioning and integration

Kinesin Eg5 as a motor protein

The kinesin spindle protein Eg5, also known as KSP or KIF11, is a significant drug target in antimitotic cancer therapy. Eg5 belongs to kinesin superfamily, and it involved in the organization and interchange of the bipolar spindle before and during anaphase. Every eukaryote has at least one Eg5, and the kinesins and other homologues include members of the kinesin subfamily (KinSin2). KRP, Kinesin-related molecular motor proteins, generates energies on microtubules for cell division and reorganization. Eg5 regulates spindle elongation during the early stages of mitosis, which aids in centrosome partitioning (Fig. 3). It is required for the formation of a bipolar spindle and the separation of sister chromatids. Effective Eg5 inhibition induces a phenotype known as the monopolar spindle, which leads to cellular mitotic seizure and apoptosis (Fig.4). There is significant genome variability in mouse models and carcinogenesis, with the effect of Eg5 overexpression. The number of Eg5 expression is few in

non-proliferating adult tissues and Eg5-focused therapy has a lower toxic profile when compared to traditional anti-mitotic therapies. Since it is highly expressed in tissues such as blood and lymphatic vascular endothelial cells, inhibiting Eg5 has two effects: anti-proliferative and anti-angiogenesis. According to the current research, the inhibition of Eg5 and associated Kinesin-5 family members continue the cause of failure of centrosome separation, spindle assembly, and bipolar spindle in the family of genes (*4*).
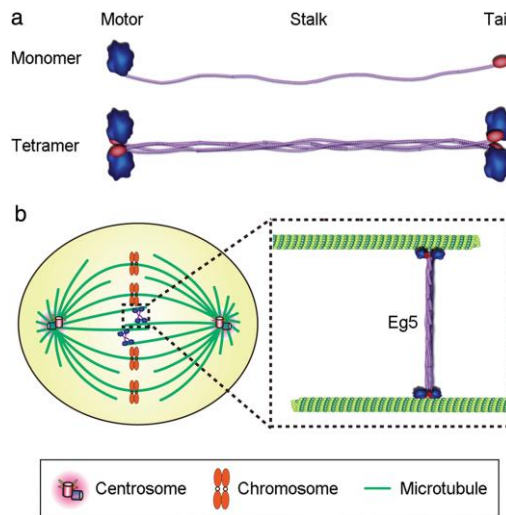
Fig. 3: The requirement of Kinesin Eg5 for the development of bipolar spindles and cell division. (Liu, M., Ran, J., & Zhou, J. (2018). Non-canonical functions of the mitotic kinesin Eg5. *Thoracic cancer*, *9*(8), 904-910.)
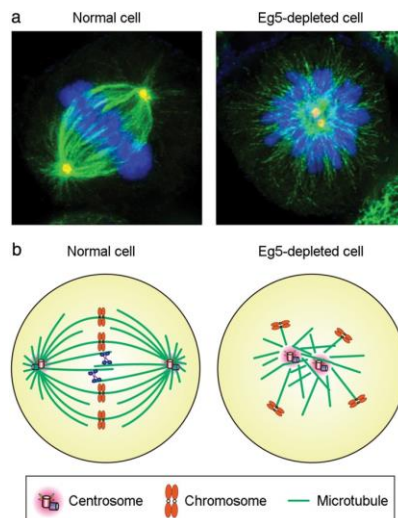
Fig. 4: Eg5 is essential for bipolar spindle formation and cell division. (Liu, M., Ran, J., & Zhou, J. (2018). Non-canonical functions of the mitotic kinesin Eg5. *Thoracic cancer*, *9*(8), 904-910.)

Loop 5 and its location

There are some motor proteins, such as Kinesin- family motors, G-protein and myosin that have developed from an ordinary ancestor protein and they allocate the Switch 1 and Switch 2 triphosphate binding domain and P- loop pattern at the nucleotide site (*5*). With a core β-sheet platform, all the mentioned three families proteins are surrounded by α-helices on both sides. P-loop is glycine- rich loop (L4) shape located between the core β3-strand and the surrounding α2 helix and is diagnosed for ATPase proteins.

Switch regions are required for the conversion of ATP chemical energy to mechanical energy. Kinesin family motors are unique in that the α2 helix is close to the P-loop and the α - helical replicate is broken to turn from the P-loop into the helix by a surface-exposed element, Loop (L5). Following L5, the α2-helix reforms and expands across the entire protein surface. The L5 function is critical in the mitotic kinesin -5 family and in transmitting information on the catalytic site to the motor mechanical element, the neck linker (NL). Several types of kinesins Eg5 inhibitors and their binding sites in L5 pocket have already been confirmed (*6*).
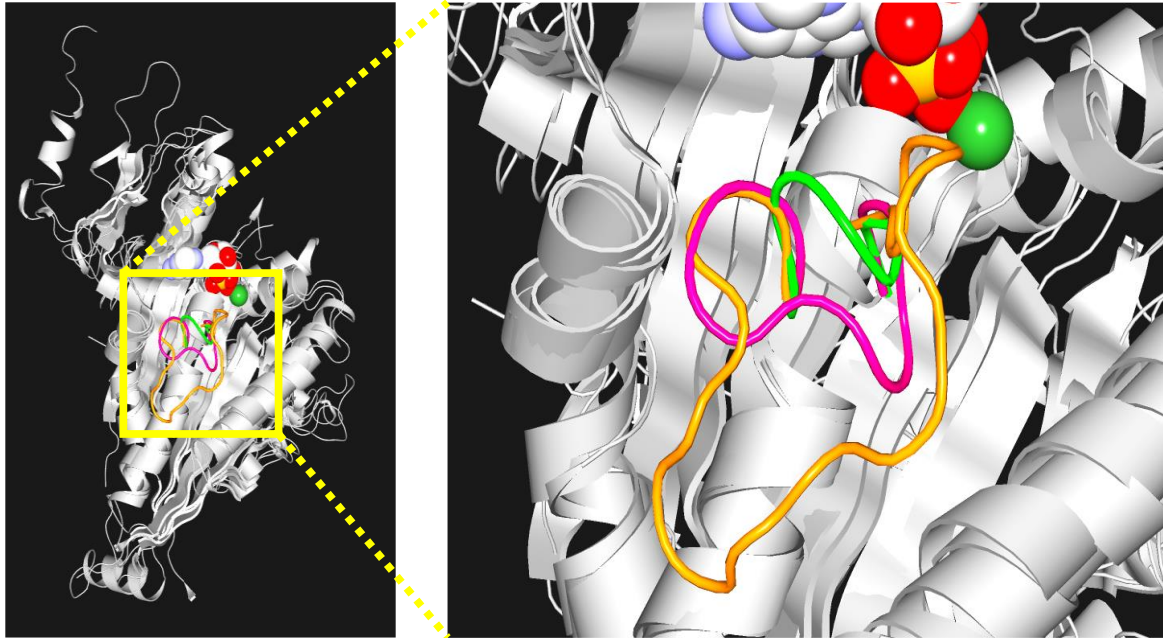
Fig.5: Difference of L5 in the crystal structure of kinesin motor domain. The crystal structure that overlay arrangements of L5 neighborhood of three kinds of kinesin. L5 of Eg5(orange), KIF5A(pink), K16(green). Loop L5 is considered to be an important functional site affecting ATP hydrolysis of kinesin and affinity with microtubules. Especially L5 of Eg5 has a very long structure unlike other kinesin and it acts as a cap of pocket and where a specific inhibitor can bind.

The mitotic kinesin Eg5 has a longer L5 with 18 amino acid residues, whereas CENP-E and conventional (kinesin-1) have shorter (7-10 residues) L5 (Fig.5). The binding interaction of inhibitors with L5 has been revealed in the presence of mitotic inhibitors such as monastrol and S-trily-L-cysteine (STLC) and abolished the activity of kinesin Eg5. As a result, it suggests that L5 has a regulating role in kinesin Eg5 motor.

Reason for targeting of antimitotic agents (Eg5 inhibitors) for cancer treatment

Antimitotic substances such as taxanes and vina alkaloids are therapeutically significant as chemotherapy drugs. These medicines work by binding to tubulin and preventing the cell cycle from progressing during mitosis by disrupting microtubule dynamics and triggering the spindle checkpoint, resulting in cell death. Tubulin is an essential cytoskeletal protein for cell division, cell shape, motility, and intracellular transports. Consequently, antimicrotubular drugs have a significant side effect of causing peripheral neuropathy by limiting axonal transport reliant on microtubules. Antimitotic drugs, as distinguished from antimicrotubular medicines, target the mitotic process (Eg5) and have been identified as a promising target for cancer therapy (*7*).

Background of kinesin Eg5 inhibitors

The first selective inhibitor of Eg5 is monastrol which induces the formation of monoastral spindles during mitosis cell division (Fig.6). The discovery of it through phenotypic screening opened a new approach for finding small compounds that impact the configuration of mitotic spindles through a machinery modification from the known antimitotic compounds. Both enantiomers of monastrol, S and R, had inhibitory effects, although the S enantiomer seemed to be stronger and induced monoastral at lower doses than the R or racemic combination (*8*).
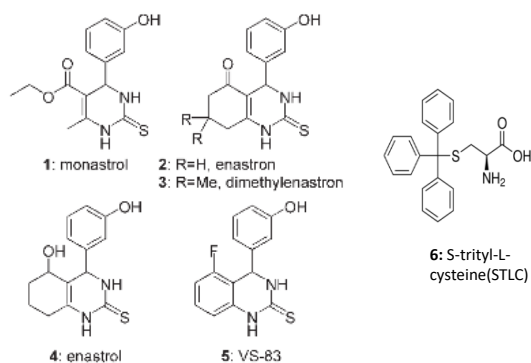
Fig. 6: Kinesin Eg5 inhibitors and their derivatives e.g. monastrol and their analogs and STLC (Sarli, V., & Giannis, A. (2006). *1*(3), 293-298.)

IC$_{50}$ value of Monastrol for inhibiting Eg5 motility is 14μM, and it causes a particular reversible block of the cell cycle. Furthermore, the allosteric inhibitory site was situated around 12Å away from the catalytical site, which was confirmed in 2004 by the effective crystallization of the inhibitor bound Eg5 complex. Several monastrol analogs have recently been produced and tested for their ability to inhibit Eg5 (Fig. 6). Monastrol regulates to conformationally restricted bicyclic complexes with enhanced inhibitory action against Eg5 due to the cyclic motion of the side chains. Enastron 2 (IC$_{50}$ = 2μM), enastron 4 (IC$_{50}$ = 2μM), and dimethylenastron have all been found as strong inhibitors (Table 2). Furthermore, the 3,4-dihydrophenylquinazoline-2 (1H)-thione structure opens the door to a novel class of Eg5 inhibitors known as vasastrols (Fig. 6). In an in vitro assay-based screen of small-molecule libraries, S-Trityl-L- cysteine was identified as an Eg5 inhibitor (Fig.6). In HeLa cells, this amino acid derivative acts as a strong Eg5 inhibitor with IC$_{50}$ values of 1.0μM.

Table 2. Inhibitors of Eg5.	
Compound	IC$_{50}$ [nM]
(S)-monastrol **1**	14000
rac-enastron **2**	2000
rac-dimethylenastron **3**	200
rac-enastrol **4**	2000
rac-VS-83 **5**	1200
terpendole E (**6**)	23000
S-trityl-L-cysteine (**8**)	1000
HR22C16 (**9**)	800
trans-tetrahydro-β-carboline **10**	90
trans-tetrahydro-β-carboline **11**	650
dihydropyrazole **13**	26
KSP-IA (**14**)	11

Source: (Inhibitors of mitotic kinesins: Next-Generation Antimitotics, Vasiliki Sarli and Athanassios Giannis, *chemMedchem 2006, 1,293-298)*

Purpose of the study

The aim of this study is the development of an inhibitor and control the function of Eg5 in the multiple states like strongly, weakly and mediumly. Previously Ishikawa, et.al. synthesized a new STLC- analog inhibitor using photochromic compounds. The inhibitor showed just two isomerization states and controlled the inhibitory activity as like as on-off photo-switch (Fig.7), (*9*). In this research, I emphasized on the formation of three isomerization states to control inhibitory activity of Eg5 more precisely. The importance of this multiple states formation is for clinical use for the treatment of cancer patients. The inhibitory activity of drug could be controlled precisely which is likely high dosage, low dosage, and medium dosages. We can control the activity of the drug, depend on the condition of the patient. For example, if the patient in severe condition, then we can apply maximum dose of drug. Subsequently, if the patient is getting better, we can minimize the drug release. Finally, if the patient getting more better, we can stop the drug release. The condition of the patient can change the activity of the drug precisely. Therefore, three stage can show appropriate activity for the condition of patient, moreover, minimize the side effects of the drugs as shown in Fig. 8.

To achieve that, I design the regulatory and inhibitory coupling (Fig.9). The regulatory part of the inhibitors is composed of photochromic compounds and the inhibitory parts are composed of the natural compounds. Interestingly, this regulatory part which is composed of photochromic compound showed inhibitory activity for Eg5 itself. Subsequently, I focused on finding out potent inhibitor of Eg5 for the inhibitory part. It has been reported that most of the Eg5 potent inhibitors are derived from synthetic sources and showed several side effects. However, to date, the inhibitor of Eg5 from natural sources has not been studied very well. Additionally, natural compounds have some advantages to use as an inhibitor and presumably,

they minimize the side effect of the drug compared to synthetic compounds. Therefore, in this study, I emphasize to discover an active compound for the inhibitory part from the natural sources which is Kolaviron as bioflavonoids, namely Garcinia biflavonoid (GB)1, GB 2, and kolaflavanone (KLF) (Fig. 10). The result of the characterization of KLF shows its inhibitory activity for Kinesin Eg5 as an inhibitor.
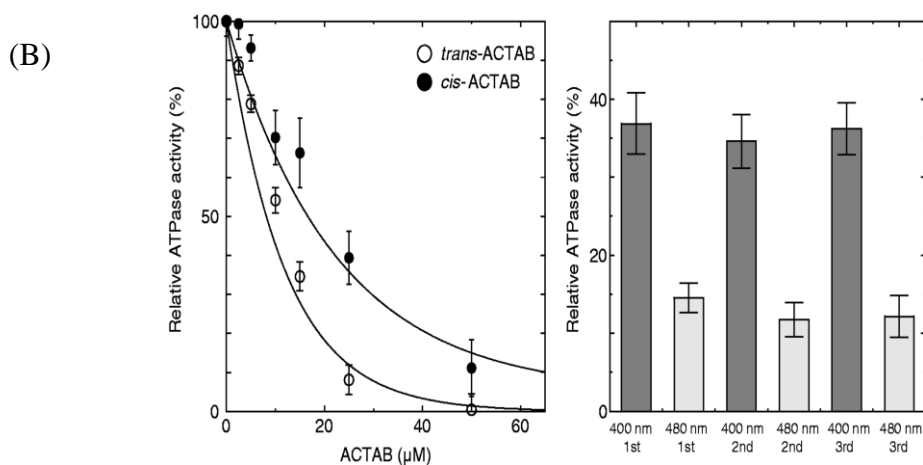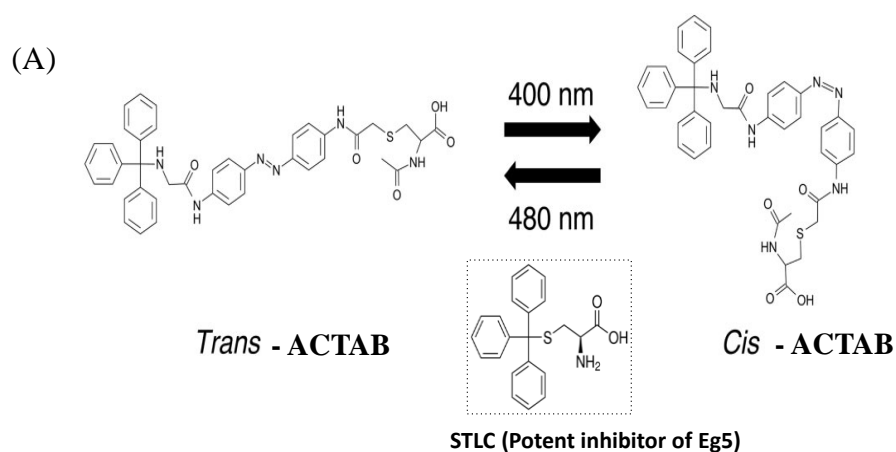
Fig. 7: (A)Photoisomerization of ACTAB. Structural formula of ACTAB. ACTAB, as an azobenzene derivative, undergoes reversible photoisomerization between the trans- and cis isomer by irradiation at 400 and 480 nm. **(B) Photocontrol of the ATPase activity of Eg5 by ACTAB.** (Source: Kumiko Ishikawa et.al. , photo-regulation of the mitotic kinesin Eg5 using a novel S-trityl-L-cysteine analogue as a photochromic inhibitor, *J.Biochem. 2014; 155(4): 257-263*)
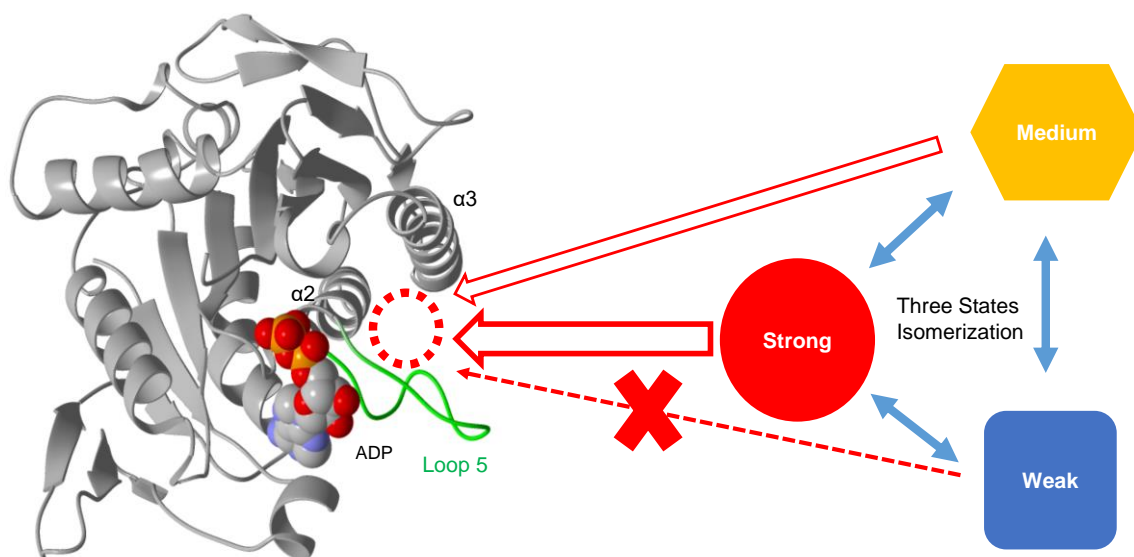
Fig.8: The aim of this study is to control the function of Eg5 using photochromic compounds which show three isomerization states.

Regulatory part (Chromic Compound e.g. photochromic compounds)

Inhibitory part (Natural sources)
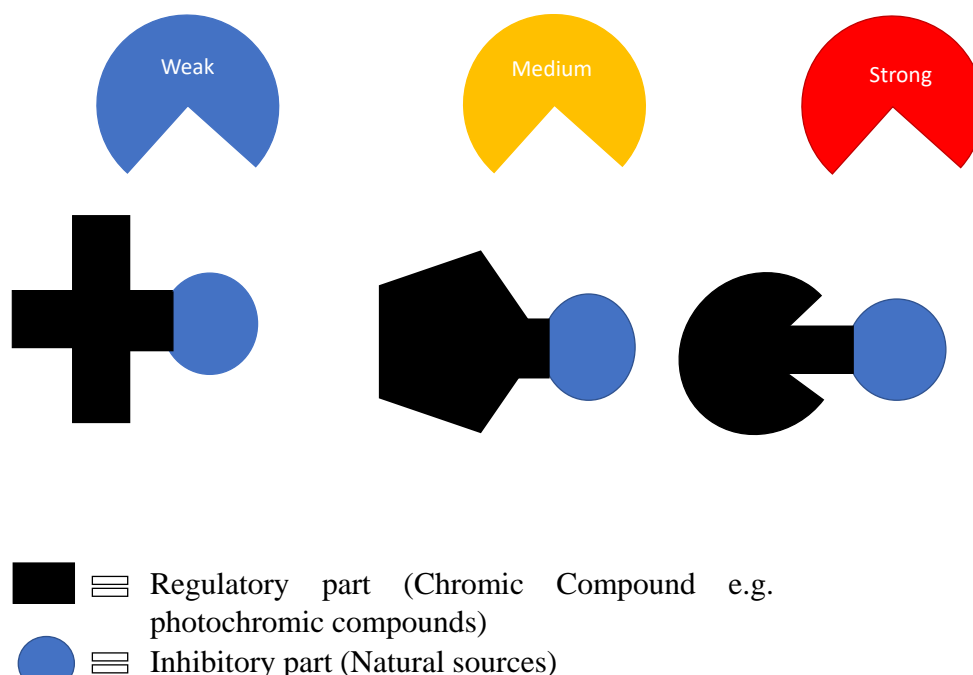
Fig.9: design and coupling the regulatory and inhibitory part for making multiple states inhibition.
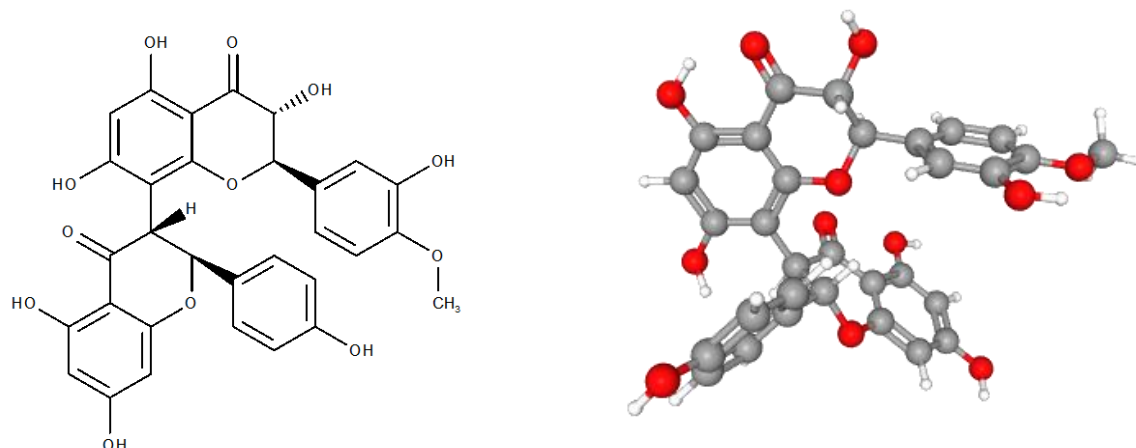
Fig. 10: Chemical structure (2D and 3D) of kolaflavanone (KLF).

Idea to control the function of Kinesin Eg5

Several findings have led to the creation of Eg5 inhibitors. Attractively, numerous small-molecules have been identified as Eg5 inhibitor, including monastrol, S-Triyl-L-Cysteine (STLC), Ispinesib, and so on. They are suitable for binding into the same druggable Eg5 allosteric pocket, which is made up of Loop L5, α2, and α3. Nonetheless, they exhibit structural variety and regulate the activity of Eg5 in a unidirectional or irreversible manner. Therefore, they could not be used as a nanodevice to reversibly regulate the functional activity of Eg5. Therefore, switching is necessary to control Eg5 activity in a reversible manner not only in general but also in functional terms. To accomplish that, I relied on chromism compounds. Chromism is a phenomenon in which external stimuli such as heat, pH, light, and the optical characteristics (color, fluorescence) and so on, affect the substance characteristics in a reversible manner. A chromic substance is a substance that shows chromism (or chromic

18

material). First, it was proposed that heat may function as a switching mechanism, like high, low, and ambient temperature. However, I utilized a protein in this experiment which is extremely sensitive to high temperatures. As a result, thermal switching is not an acceptable approach.

Following that, I emphasized on the creation of switching with various pH levels, such as acidic, alkaline, and neutral. However, both acidic and alkaline pH are detrimental to the protein's overall structure. As a result, pH might not be suitable for using as a switch. Eventually, I worked on light to develop switching using photochromic compounds. Photochromic chemicals are widely recognized for their light sensitivity.

Photochromic compounds and its function

Photochromic compounds are those compound that change the structure and properties reversibly in response to photo stimulation. Photochromism is defined by IUPAC as a "light-induced reversible change of color". It has been reported that the photochromic compounds act as molecular switch in the biological system. The organic photochromic molecular switch could be reversely interconverted depend upon the reactions stimulated by light excitation and varied absorption spectra. These two characteristics change likewise in various other physical properties such as fluorescent intensity, acid/base strength, dipolar moment, molecular shape, and so on. In photochemistry, several altered organic photochromic molecules are well known such as azobenzenes, stilbenes, spiropyranes, fulgides, diarylethenes and chromenes among many others (Fig. 10). There are three altered categories such as trans-cis-trans isomerizations, photo-induced ring closing reaction and photo-tautomerism that are formed in the photochromic processes (*10*).

The photochromic systems are categorized into two categories, based on the thermal stability of the photogenerated isomer. At the elevated temperatures, the isomers that do not return to its initial isomers referred as **P-type** (photochemically reversible type). For example: fulgides and diarylethenes. The photogenerated isomer thermally returns to its actual form as referred as **T-type** (thermally reversible type). For example: Azobenzenes, Stilbenes or spiropyranes (Fig.10).
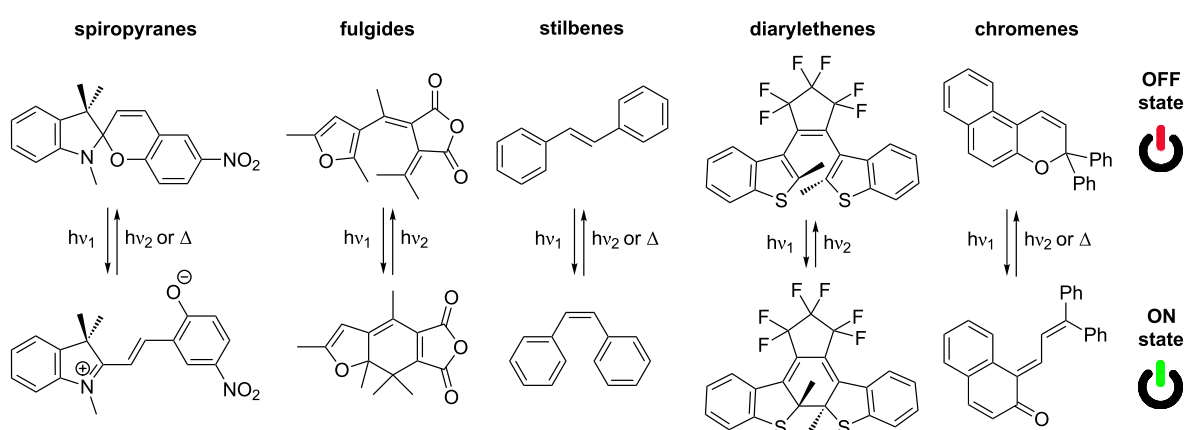
Fig. 11: A list of photochromic molecules and their isomer formation (García-Amorós, J., & Velasco, D. (2012). Recent advances towards azobenzene-based light-driven real-time information-transmitting materials. *Beilstein journal of organic chemistry*, *8*(1), 1003-1017)

Chapter 2

Novel photochromic inhibitor for mitotic kinesin Eg5 which

forms multiple isomerization states

Introduction

Kinesins are a superfamily of molecular motors that play a key role in an assortment of physiological capacities by transporting intracellular cargos along microtubule (MT) filaments. In some cases, represented as "nano-machines", kinesins alter the chemical energy of ATP into mechanical force, driving their cargo towards the termination of the MT in most cases (*11*). In the human genome, 45 different kinesins have been reported based on their specific amino acid of the motor domain and are related to various diseases. There are a few kinesins that play a fundamental part in the cell cycle (*12*). Among the entire superfamily, Kinesin Eg5, which is also referred to as KSP or KIF11, has been properly studied due to its physiological properties in eukaryotic cells. Most of the important functions of kinesin Eg5 include transportation of molecular cargos, neurotransmitters, axon transport, and bipolar spindle formation during eukaryotic cell division. Effective obstruction of Eg5 function stimulates a hallmark phenotype known as the monopolar spindle and leads to cellular mitotic seizure and apoptosis (*13,14*). Therefore, Eg5 has been considered as a target for cancer therapy, and inhibitors specific for Eg5, such as Monastral, STLC Ispinesib, SB-743921, and ARRY-520, have been developed. Interestingly, although their structures are not conserved, they target the same binding pocket composed of helix α2, α3, and loop L5, located around 10 Å away from the ATPase site (*15*).

In our laboratory, we have been trying to develop functional novel inhibitors of Eg5 with photo switching inhibitory activity. It was reported that the aromatic ring resembled the Eg5 inhibitor and photochromic molecules. It is expected to apply to photo-switching of the Eg5 inhibitor. In a previous study, it was demonstrated that the modification of the functional region L5 in the Eg5 motor domain using photochromic compounds showed photocontrol of Eg5 ATPase activity (*16*). However, the chemical modification of Eg5 with photochromic compounds to accomplish photocontrol has not been adjusted for application in living cells. Therefore, we focused on developing and synthesizing novel inhibitors using photochromic

compounds that can permeate the cell membrane and control the Eg5 activity photo-reversibly in living cells.

Photochromic compounds are compounds that change the structure and properties reversibly in response to photo stimulation. It has been reported that photochromic compounds act as molecular switches in biological systems. Photochromic systems are categorized into two types based on the thermal stability of the photogenerated isomer. At elevated temperatures, the isomers that do not return to their initial isomers are also referred to as P-type (photochemically reversible type) isomers, for example, fulgides and diarylethenes. The photogenerated isomer thermally returns to its actual form, as referred to as T-type (thermally reversible type), for example, azobenzenes, stilbenes, or spiropyranes (*17*). Photochromic azobenzene is photo-isomerized to a hydrophilic Cis-isomer by UV light and a hydrophobic trans isomer by visible light (VIS) irradiation (*(18-21)*). On the other hand, Spiropyran exhibited open ring zwitterion containing photo-isomer Merocyanine form under UV light and close ring hydrophobic Spiro form beneath VIS light *(22)*.

Ishikawa, et.al. synthesized a novel STLC- analog inhibitor using photochromic compounds. The inhibitor showed two isomerization states and different inhibitory activities such as on-off the photo-switch photo-reversibly. Sadakane, et.al. designed and synthesized another couple of novel inhibitors composed of the double photochromic compounds Spiropyran or Azobenzene. The inhibitors also displayed two isomerization forms and inhibited Eg5 ATPase and motility activities at two levels, efficiently correlating with the photo-isomerization among the two states (*23-25*). Generally, each photochromic compound exhibits two photo-isomerization states by light irradiation photo reversibly. Theoretically, combining two different kinds of photochromic molecules enables the formation of more than two isomerization states. The three state formations are of clinical significance in the treatment of cancer patients. The inhibitory activity of drugs could be controlled precisely, which is likely

to be high dosage, low dosage, and medium dosages, considering the condition of the patients (**graphical abstract**).

Kinesin Eg5   *Multi-isomerization Photochromic inhibitor*
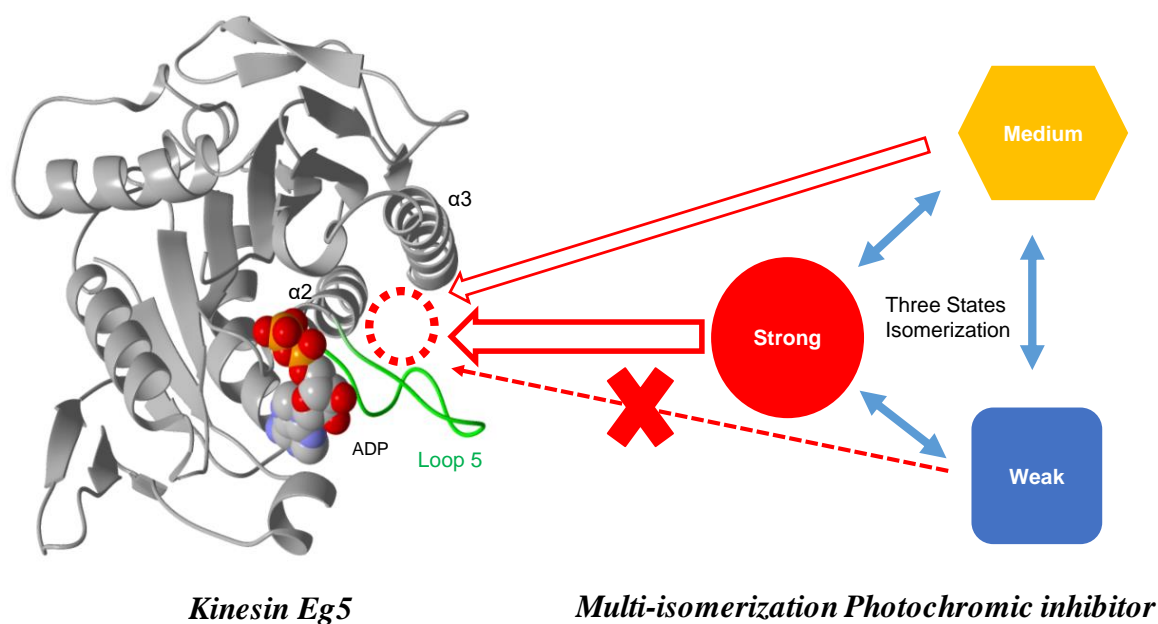
Schematic representation of the proposed multiple photo regulation by the novel photochromic inhibitor which exhibits three isomerization states. Photocontrol of kinesin Eg5 by multi-

In this study, I employed two photochromic compounds, Spiropyran and Azobenzene, to synthesize Eg5 inhibitors that exhibit multiple levels of inhibitory activity for Eg5. In fact, the novel photochromic inhibitor showed three isomerization states and three inhibitory activities for Eg5 by photo-stimulation. It is anticipated that the novel photochromic inhibitor will be able to accomplish the photocontrol of mitotic cell division and bring a notable change beyond the current anticancer therapy.

Materials and Method

Synthesis of photochromic inhibitors (SPSAB) composed of spiropyran and sulfonated azobenzene

The photochromic inhibitor, spiropyran-sulfonated azobenzene (SPSAB) was synthesized. The significance of SPSAB inhibition is hydrophilicity. The synthesis of hydrophilic SPSAB involves the coupling reaction of 1-(β-carboxyethyl)-3′, 3′-dimethyl-6–nitrospiro (indoline-2′, 2 (2H-1) benzopyran) (SP-COOH) and 4-Aminoazobenzene-4'-sulfonic Acid Sodium Salt with coupling reagents 1-ethyl-3-(3-dimethylaminopropyl)-carbodiimide (EDC) and 1-Hydroxy-7-azabenzotriazole (HOAt). Prior to the coupling reaction, an activated SP ester was prepared. SP-COOH (65.72 μmol) was activated with EDC (78.86 μmol) and HOAt (65.72 μmol) for 10 min in 1.0 mL dry N, Ndimethylformamide (DMF) at room temperature (RT), and stirred with a magnetic stirrer. Subsequently, 4-Aminoazobenzene-4'-sulfonic acid sodium salt was added to the mixture of activated SP ester and reacted overnight at room temperature (RT). The expected hydrophilic inhibitor was purified in a large TLC (PLC silica gel60, MERCK) and used as a developing solvent of 20% methanol and 80% chloroform and extracted with 100% methanol using a rotary centrifuge at 8000 rpm, 20ºC, 15 min. The Rf value of SPSAB was 0.31. Finally, the synthesized inhibitor SPSAB was confirmed using a fast atom bombardment mass spectrum (FABMS) and showed a molecular ion at m/z 638+1. This corresponds to a molecular mass of 639.678 as calculated from the formula of SPSAB.

Photo-isomerization of SPSAB

Three isomerization states of SPSAB were irradiated at 366nm using a black - ray lamp (16W, UVP, Upland, CA, USA), visible light (VIS) using a fluorescent lamp (27W), and in the dark to convert SP-trans - SPSAB to MC- cis- SPSAB, MC- cis -SPSAB to SP-trans - SPSAB, and finally, MC- cis -SPSAB to MC- trans- SPSAB. In the solution of 30 mM Tris- HCl (pH 7.5), the isomers of SPSAB were dissolved and the light was irradiated from 5 cm above surface of the solvent at 25^{0}C.

Expression and purification of the mitotic kinesin Eg5 motor domain

The motor domain of Eg5 was prepared as per the following revised method. Wild-type mouse Eg5 (WT, amino residue 1-367) that contains cDNA of the motor domain was enlarged using the polymerase chain reaction (PCR) and ligated into the pET21a vector. *Escherichia coli* BL21(DE3) (Invitrogen, CA, USA) was transformed with Eg5 WT and the mutant expression plasmids. *Escherichia coli* was cultured for 2.5 h at 37 °C in 3L of LB medium with 100 µg/mL amipicillin till the optimal culture density reached at 600nm. The addition of 0.5 mM isopropyl β-D thiogalacto-pyranoside (IPTG) solution induced the expression of Eg5 mutants. The incubation was sustained for 18 h at 18 °C. At 4 °C for 15 min, the cells were harvested by centrifugation at 5000×g using a No. 30 rotor (Hitachi Himac CR22G). The precipitate was suspended in HEM buffer (10mM 4-(2-hydroxyethyl)-1-piperazineethane-sulfonic acid [HEPES], pH 7.2, 1mM $MgCl_2$, 1mM [ethylenebis (oxyethylenenitrilo)]tetraactic acid [EDTA], and 25 mM NaCl) and then stored at − 80 °C.

At 4°C, purification was performed. The frozen cells were thawed, suspended in 15 mL of sonication buffer (20mM MOPS pH7.0, 500mM NaCl, 1mM $MgCl_2$, 0.2mM β-mercaptoethanol, 0.5mM phenylmethylsulfonyl fluoride (PMSF), 2 µg/mL leupeptin, 2 µg/mL aprotinin, and 2 µg/mL pepstatin A), and later sonicated for 5 cycles (sonication for 30s and

on ice for 30s) with an ultra-S homogenizer (VP-305, taitec, Saitama, Japan) at a micro tip limit of 5-6 and a duty cycle of 50%. The cell lysate was centrifuged at 235,000×g for 1 h using a 45Ti rotor (Beckman Coulter, CA, USA Optima XL-90 ultracentrifuge), and the supernatant was applied to a Co- nitrilotriacetic acid (NTA) column (Talon Metal Affinity Resin, Takara, Shiga, Japan). The Co-NTA column was utilized to purify the Eg5 WT. Using lysis buffer containing 150 mM imidazole, Eg5 was eluted from the Co-NTA column. Sodium dodecyl sulfate polyacrylamide gel electrophoresis (SDS-PAGE) was used to examine the fractions and confirm the molar mass of Eg5 (43kD). Purified Eg5 was dialyzed in buffer (30 mM Tris-HCl at pH 7.5, 120 mM NaCl, 2.0 mM $MgCl_2$, 0.1 mM ATP, and 0.5 mM DTT) and stored at -80ºC.

Purification and polymerization of tubulin

According to the method described by Hackney, tubulin was purified from porcine brains. At 37 °C, tubulin was polymerized for 30 min in 100 mM PIPES (pH 6.8), 1.0 mM EGTA, 1.0 mM $MgCl_2$, and 1.0 mM GTP. Further, taxol was added to a final concentration of 10 µM. At 37 °C, the polymerized microtubules were collected by centrifugation at 80,000 rpm for 15 min. The microtubule pellet was collected in a buffer comprising 100 mM PIPES (pH 6.8), 1.0 mM $MgCl_2$, 1.0 mM GTA, and 10 µM Taxol, excluding the supernatant.

Kinesin ATPase assay

The ATPase assay was implemented as per the methodology mentioned previously. By using 20 mM HEPES (pH 7.2), consisting of 50 mM KCl, 2 mM $MgCl_2$, 0.1 mM EDTA, 0.1 mM EGTA and 1.0 mM β-mercaptoethanol, the activity of kinesin ATPase was measured. SPSAB dissolved in DMF was irradiated using UV light, visible light (VIS), and in the dark and added to the assay buffer at a final concentration of 0.0-150 µM, to analyze the effect of the photo-isomerization of the inhibitor. The ultimate DMF concentration in the Eg5 ATPase buffer was 5.0%. Excluding the microtubules, 0.5 µM Eg5 was added to the assay buffer for

basal ATPase activity. About 0.1 µM Eg5 motor domain was added to the assay buffer in the presence of a 3.0 µM microtubule solution for microtubule-stimulated ATPase activity. The ATPase reaction was initiated by adding 2.0 mM ATP and concluded by adding 10% trichloroacetic acid (TCA). The stipulated time for the reaction of microtubule-stimulated ATPase or basal ATPase activity was 10 or 30 min at 25°C. The released inorganic phosphate (Pi) in the supernatant was measured according to the method of Youngburg.

Motility assay

As previously mentioned, the methodology is slightly altered to perform the *in vitro* motility assays (13). In the assay buffer (10mM Tris-acetate, pH7.5, 50 mM potassium-acetate, 2.5 mM EGTA and 4.0 mM $MgSO_4$), the coverslips were coated with an anti-6x histidine monoclonal antibody (Wako). Consequently, the chambers were incubated at 25 °C for 2 min and 0.5 µM Eg5 in assay buffer A (10mM Tris-acetate, pH7.5, 50 mM potassium-acetate, 2.5 mM EGTA, 4.0 mM $MgSO_4$, and 0.2% β-mercaptoethanol) was perfused through the flow of chambers. After cleaning the chambers with assay buffer, A, 1.0 mg/mL casein in assay buffer A was perfused through the flow chambers, and the chambers were incubated for 5 min at 25°C. Simultaneously, 110 µM photo isomerized SPSAB, which was irradiated with VIS light, UV (366 nm) for 10 min, and in the dark for 21 h in assay buffer A, was perfused through the flow chambers and the anchored Eg5 was treated for 2 min at 25°C. Later, the rhodamine-labeled microtubules in assay buffer B (assay buffer A with 110 µM photo-isomerized SPSAB and 20.0 µM taxol) were perfused through the flow chambers. Next, assay buffer B was used to wash the chambers. Conclusively, 1.0 mM ATP and 110 µM photo isomerized SPSAB in assay buffer C (assay buffer B with 1.5 mg/mL glucose, 0.01 mg/mL catalase, and 0.05 mg/mL glucose oxidase) were perfused through the flow chambers. The ultimate DMF concentration

in the assay buffer was 5.0%. An Olympus BX50 microscope equipped with a CCD camera was utilized to view the rhodamine-labeled microtubules.

Mixed motor gliding assay

The same procedure has been followed as mentioned in the mobility assay.

Results

Design, synthesis, and photo-isomerization of Eg5 inhibitors SPSAB, which form three states

I employed a photochromic compound combination of azobenzene and spiropyran to create a photochromic inhibitor that exhibits multiple inhibitory activities for kinesin Eg5. Previously, it has been reported that the homodimer of azobenzene or spiropyran derivatives worked as a potent photochromic inhibitor. Therefore, the heterodimers of azobenzene and spiropyran are also expected to show inhibitory activity. SP-COOH was coupled with 4-Aminoazobenzene-4'-sulfonic acid according to the established methods described in the Methods and Materials section. The incorporation of sulfonic acid is expected to increase the solubility in physiological solutions. Azobenzene isomerizes between cis and trans, and spiropyran exhibits spiro and merocyanine isomers. Therefore, the SPSAB composed of azobenzene and spiropyran can theoretically form four isomerization states, SP-trans, SP-Cis, MC-cis, and MC-trans (Fig.12). Isomerization among the combined isomers of SPSAB induced by light irradiation or in the dark condition were monitored by absorption spectra. It is well known that the absorption spectral change of spiropyran accompanied by SP-MC isomerization occurs at 530 nm. On the other hand, cis-trans isomerization of azobenzene induces an absorption spectral change at 350 nm (*26,27*). Isomerization of SPSAB induced by UV or VIS light irradiation was monitored by measuring the absorption spectral changes. Visible light irradiation induced an increase in absorption at 350 nm and decreased at 530 nm, as shown in Fig. 13A, reflecting the SP-trans isomerization state. Subsequently, UV irradiation decreased the absorption at 350 nm and increased the absorption at 500 nm corresponding to the formation of the MC-cis isomerization state (Fig. 13B). The absorption of spiropyran at 350 nm and UV and VIS light irradiations induce slight absorption changes correlating with

SP-MC isomerization, as shown in Fig. 14. Therefore, the significant absorption changes at 350 nm of SPSAB composed of spiropyran and azobenzene upon light irradiation is due to Trans-Cis photo-isomerization of the azobenzene moiety (Fig. 13A and B).
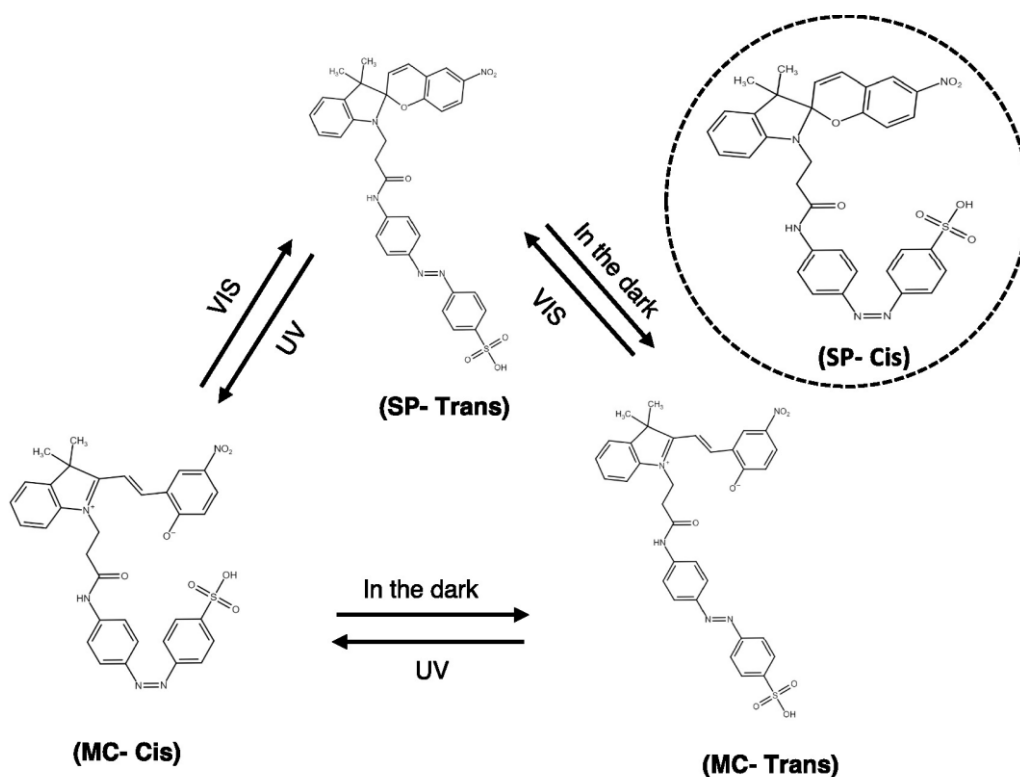
Fig. 12: Photo-isomerization of the Spiropyran- Sulfonated Azobenzene (SPSAB). The newly designed and synthesized photochromic inhibitor SPSAB for kinesin Eg5 was composed of spiropyran and sulfonate groups containing azobenzene. Theoretically, it had the possibility to show four possible isomerization states like SP-trans, SP-Cis, MC-trans and MC-cis. However, practically in the physiological condition, just three isomerization states were achieved, such as SP- Trans, MC-cis and MC- Trans by the Visible light (VIS), Ultraviolet (UV) light irradiation or incubation in the dark, respectively, as shown in this figure.

Interestingly, the spiropyran moiety of SPSAB exhibited reverse photochromism in the dark at 30 mM Tris- HCl (pH 7.5) buffer, resulting in the formation of the third isomerization MC-trans state (Fig. 13C). However, I could not achieve SP-cis isomerization by light irradiation or other stimulations under physiological conditions. From the spectral changes, I demonstrated the three combined isomerization states of SP-trans, MC-cis, and MC-trans by light irradiation or incubation in the dark.
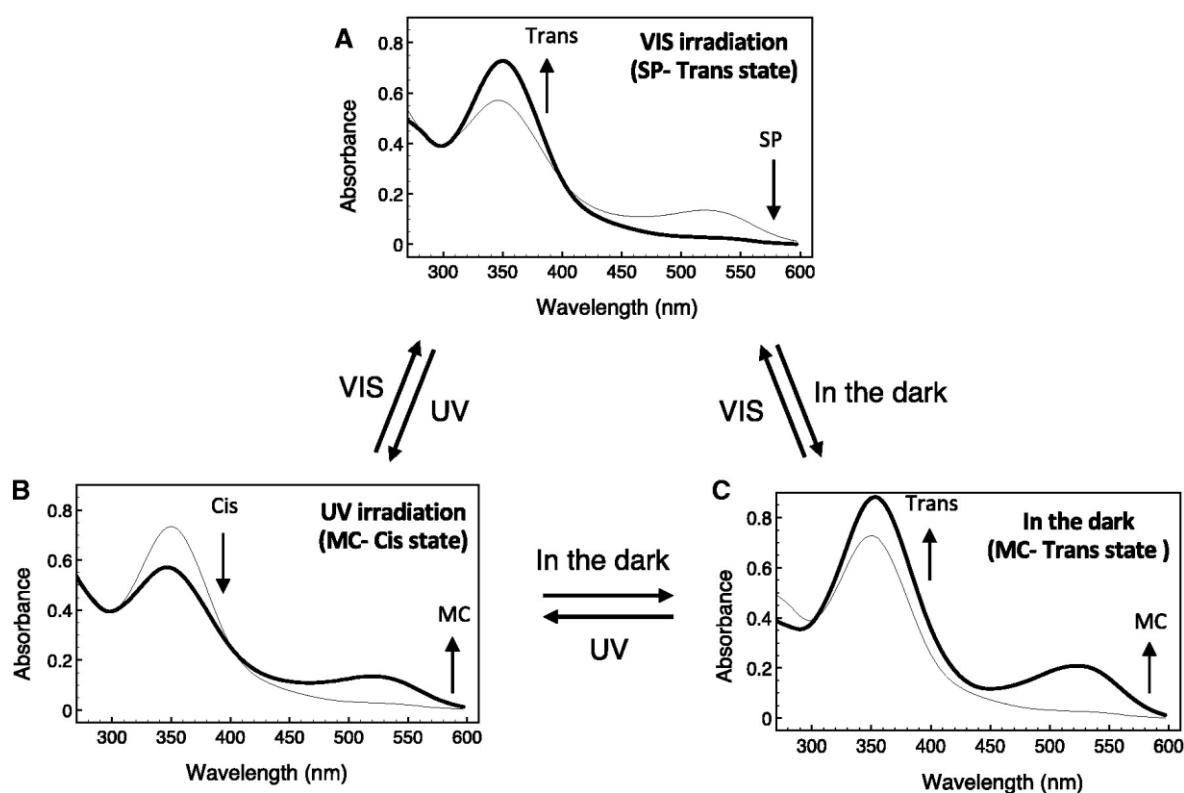
Fig. 13: Measuring the change of absorbance spectrum of synthesized SPSAB. Three isomerization states of SPSAB were formed to illustrate SP- Trans (VIS), MC- Cis (UV) and MC- Trans (In the dark) respectively. In this experiment, 78 µM SPSAB was dissolved in 30 mM Tris HCl (pH 7.5) and the absorption spectrum was measured under visible light, UV light (366 nm) and in the dark respectively. (A) In the visible light condition (irradiation time 0-15 min), it formed SP-trans isomerization, and a peak appeared around 350 nm. (B) Under UV

(irritation time 0-15 min), it became MC-cis isomerization, and the peak was appeared around 530 nm. (C) Finally, in the dark (irradiation time 0-21 h), it became an MC-trans isomerization, and the peaks appeared around 350 nm and around 530 nm. Typical three-state absorption spectra were observed.
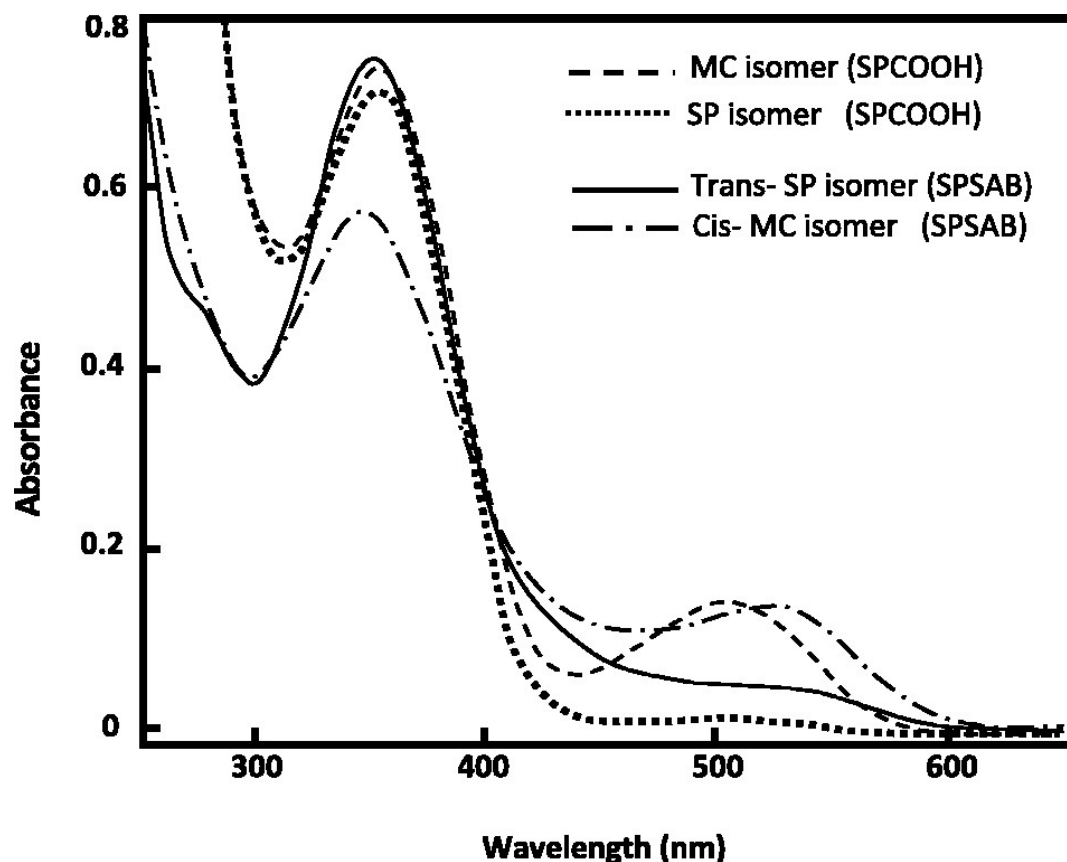
Fig. 14: Comparison of the spectral changes of SPCOOH and SPSAB correlating with isomerization. It was compared to confirm the spectrum change of Sulfonate Azobenzene with SP-COOH and SPSAB. In this figure, dash line (-----) and dotted line (······) indicate Merocyanine (MC) and Spiro (SP) SP-COOH. On the other hand, plain line (——) and dash dotted line (— · —) indicate Trans and Cis isomer of SPSAB. It is clear that the dash line and the dotted line overlap with each other at 350 nm. However, the plain line and the dash dotted line showed significant changes between them. Therefore, the difference in the spectrum from the plain line to the dash dotted line indicate the isomerization change from Cis to Trans or from Trans to Cis for azobenzene derivatives.

Photo-control of the SPSAB inhibitory activity on the basal Eg5 ATPase

The inhibitory activities of SPSAB in the three isomerization states of SP-trans (VIS), MC-cis (UV), and MC- trans (in the dark) were examined on the basal ATPase activity of Eg5 without microtubules. As shown in Fig. 15A, the three SPSAB isomers inhibited basal ATPase activity in a concentration-dependent manner with different inhibitory activities. The half-maximal inhibitory concentrations (IC_{50}) for the three isomerization states were estimated. The SP-trans isomer showed the highest inhibitory activity at an IC_{50} value of 30 µM. In contrast, MC-cis had the lowest IC_{50} value of 86.0 µM among the three isomers. The IC_{50} of MC-trans was 38.7 µM and the middle value between SP-trans and MC-cis. It was demonstrated that each isomer of SPSAB exhibits Eg5 basal ATPase activity with different inhibitory activities.
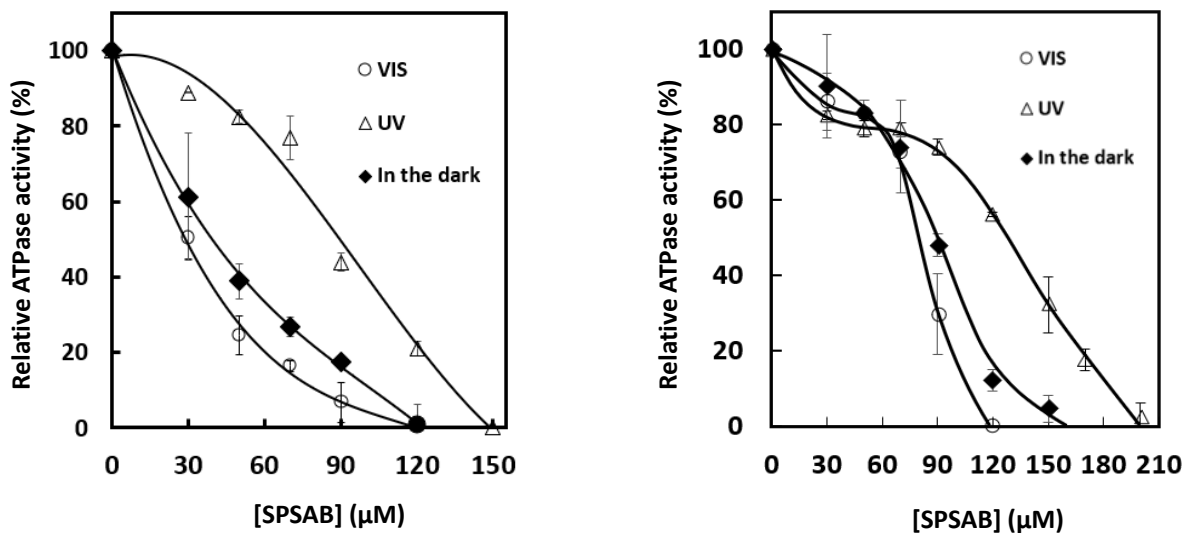
Fig. 15: Photo-regulation of Kinesin Eg5 ATPase using three state isomerization of SPSAB. (A) Dose-dependent inhibition of basal Eg5 ATPase activities by SP-trans (◯), MC-cis (△), and MC-trans (◆) of SPSAB (0-150 µM) in 0.5 µM Eg5, 20 mM HEPES-KOH (pH 7.2) containing 50 mM KCl, 2 mM $MgCl_2$, 0.1 mM EDTA, 0.1 mM EGTA and 1.0 mM β -mercaptoethanol, and 2.0 mM ATP at 25°C, 15 min. **(B)** Dose-dependent inhibition of MT

dependent Eg5 ATPase activities by SP-trans ($\bigcirc$), MC-cis ($\triangle$) and MC-trans ($\blacklozenge$) of SPSAB

(0-200 µM) in 0.1 µM Eg5, 3 µM MT, 20 mM HEPES-KOH (pH 7.2) containing 50 mM KCl, 2 mM MgCl$_2$, 0.1 mM EDTA, 0.1 mM EGTA and 1.0 mM B-mercaptoethanol, and 2.0 mM ATP at 25°C, 15 min. Results of the three independent experiments are presented as mean ± SD (error bar).

Photo-control of the SPSAB inhibitory activity on microtubule-stimulated Eg5 ATPase

I also examined the inhibitory activity of SPSAB on microtubule (MT) - stimulated ATPase activity among the three states. As shown in Fig. 15B, microtubule-stimulated ATPase activity was also inhibited by the three SPSAB isomers in a concentration-dependent manner with different inhibitory activities for each isomer. Interestingly, for all three isomers, concentration-dependent inhibitory activities exhibited bi-phase alterations. At lower concentrations of SPSAB from 0 to 60 µM, there was a slow decrease in ATPase activity. On the other hand, at more >60 µM, a rapid decrease in ATPase was observed, accompanied by an increase in the concentration of SPSAB. The first phase may be due to the binding of SPSAB to the subsite, where it has a relatively high affinity for SPSAB but has no influence on the ATPase activity by binding of SPSAB. At higher concentrations of SPSAB, the three isomerization states clearly showed different inhibitory activities in a dose-dependent manner. The order of the inhibitory activities among the three was the same as the inhibitory activities in the basal ATPase. The most potent inhibitory activity was shown by the SP-trans isomerization state at an IC$_{50}$ value of 79.1 µM. The IC$_{50}$ of the MC-trans and MC-cis isomers were 83.3 µM and 121.5 µM, respectively. The effective three-step photocontrol of Eg5 activity was achieved by the isomerization of SP- trans, MC- cis, and MC- trans of SPSAB in the range of 90-120 µM.

The influence of SPSAB on the interaction between Eg5 and MTs was also examined. I measured the MT concentration-dependent ATPase activity of Eg5 in the presence of the three isomerization states of SPSAB. The V_{max} values of the three isomers were almost the same, ~60% of V_{max} in the absence of SPSAB. SP-trans showed a slightly higher V_{max} than the other two states, as shown in Table 3. On the other hand, the three isomers clearly exhibited different K_{MT}s, as shown in Table 3. The SP-trans isomer significantly decreased Eg5 affinity for MTs with a K_{MT} of 5.5 μM. Interestingly, ATPase inhibition of dose dependent MTs with the SP-trans isomer showed a sigmoidal shape (Fig.16). Previously, the similar phenomena observed on the Eg5 inhibitor composed of the two spiropyran molecules, DSPPA (*25*). The sigmoidal shape may be induced by the spiropyran moiety of SPSAB.

Table 3. Calculation of V_{max} and K_{MT} values of Eg5 ATPase in the presence of three isomerization states of SPSAB

Inhibitors (isomerization)	V_{max} (s^{-1})	K_{MT} (μM)
Control (DMF)	10.24 ± 0.36	1.58 ± 0.2
MC-*cis* (UV)	6.63 ± 0.6	2.53 ± 0.6
MC-*trans* (in the dark)	6.78 ± 1.97	4.51 ± 2.25
SP-*trans* (VIS)	7.1 ± 0.86	5.9 ± 0.65
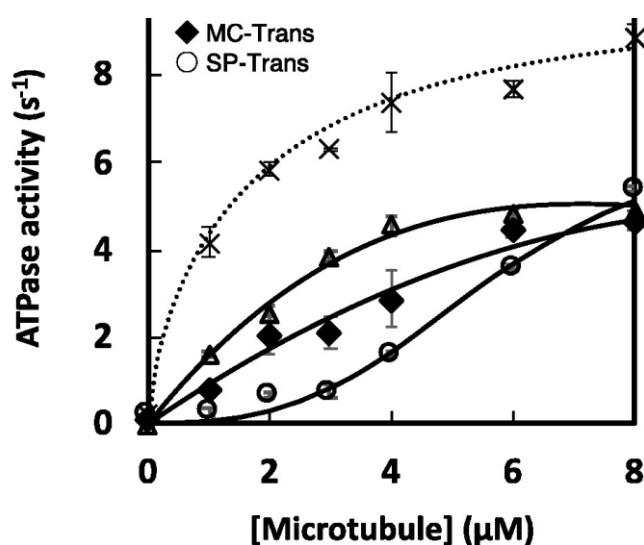
Fig. 16: Microtubule-stimulated ATPase activity in the presence of three isomerization states. Inhibitory effect of SPSAB photoisomers on the interaction between Eg5 and microtubules. The microtubule dose-dependent ATPase activities in 0.1µM Eg5, 0-8 µM microtubule, 20 mM HEPES-KOH (pH 7.2), 50 mM KCl, 2 mM MgCl$_2$, 0.1 mM EDTA, 0.1 mM EGTA, 1.0mM β-mercaptoethanol, 2.0 mM ATP, 5% DMF in the presence of 110 µM of SP-trans (○),MC-cis (△) and MC-trans (◆) of SPSAB and in the absence of SPSAB (×).

From the data, it concluded that the optimal conditions for SPSAB to control the MT-dependent ATPase activity as a three-step photo-switch is 90-120 µM SPSAB in the presence of 2-4 µM MTs (Figs 15B and 16).

Photo- regulation of Eg5 motor activity with SPSAB

I also examined the effect of the three SPSAB isomers on Eg5 motor activity. An *in vitro* motility assay using fluorescently labeled microtubules was performed according to established methods as described in the Materials and Methods section. The gliding velocity of the MTs on the Eg5 adsorbed glass surface in flow cells was measured in the presence of the three isomers. In the absence of the SPSAB isomer (control), the average MT gliding velocity was 10.78±1.47nm/s, as shown in (Fig.17A). In the presence of the SP-trans isomer, the average velocity of MTs clearly slowed down to 8.47±1.1nm/s (Fig. 17B). The histogram of the velocity in the presence of MC-cis showed a slightly broader distribution in the range from control to SP-trans with the MTs gliding average velocity being 10.01±1.78 nm/s, as shown in Fig. 17C. The MC-cis isomer showed a middle value of average velocity of 9.56±0.5 nm/s compared with those of the other two isomers.

The experimental data clearly suggest that the ATPase and motility activities of mitotic kinesin Eg5 are controlled photo reversibly by the novel photochromic Eg5 inhibitor SPSAB, which exhibits three different isomerization states.
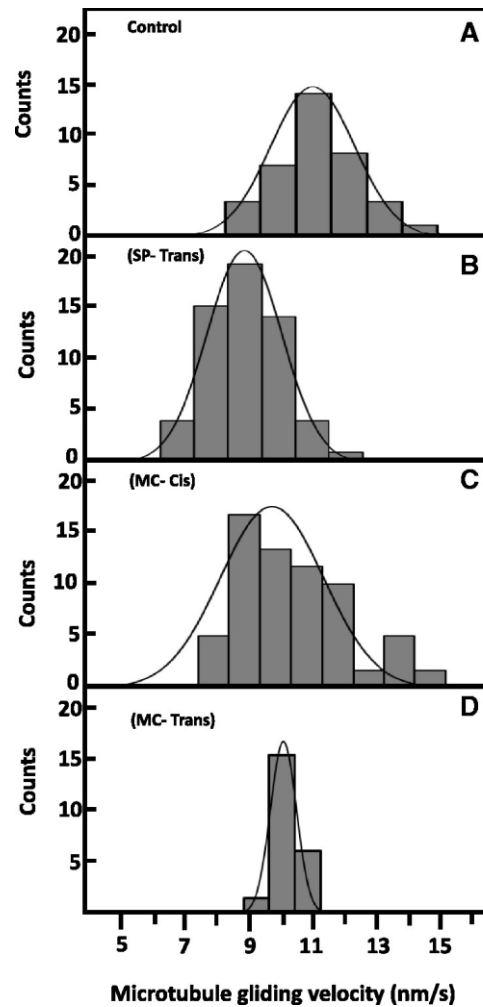
Fig. 17: Observation of the effect of SPSAB on Eg5 motor activity using fluorescence microscopy *in vitro* motility assay. (A) In the absence of SPSAB (Average velocity 10.781 ± 1.47 nm/s, n=33); (B) In the presence of 110 µM SP- trans (SPSAB) (Average velocity 8.47 ± 1.1 nm/s, n=62; (C) In the presence of 110 µM MC- cis (SPSAB) (Average velocity 10.01 ± 1.78 nm/s, n=44); and (D) In the presence of 110 µM MC- trans (SPSAB) (Average velocity 9.56 ± 0.5 nm/s, n=17).

Mix motor gliding assay

In the presence of both kinesin 1 and Eg5, the mixed motor gliding assay was done (Fig.18). In the mix motor assay, the velocity of Kinesin 1 was 10-fold faster than the kinesin Eg5. However, Kinesin Eg5 has a crucial role to increase or decrease the velocity of Kinesin 1.
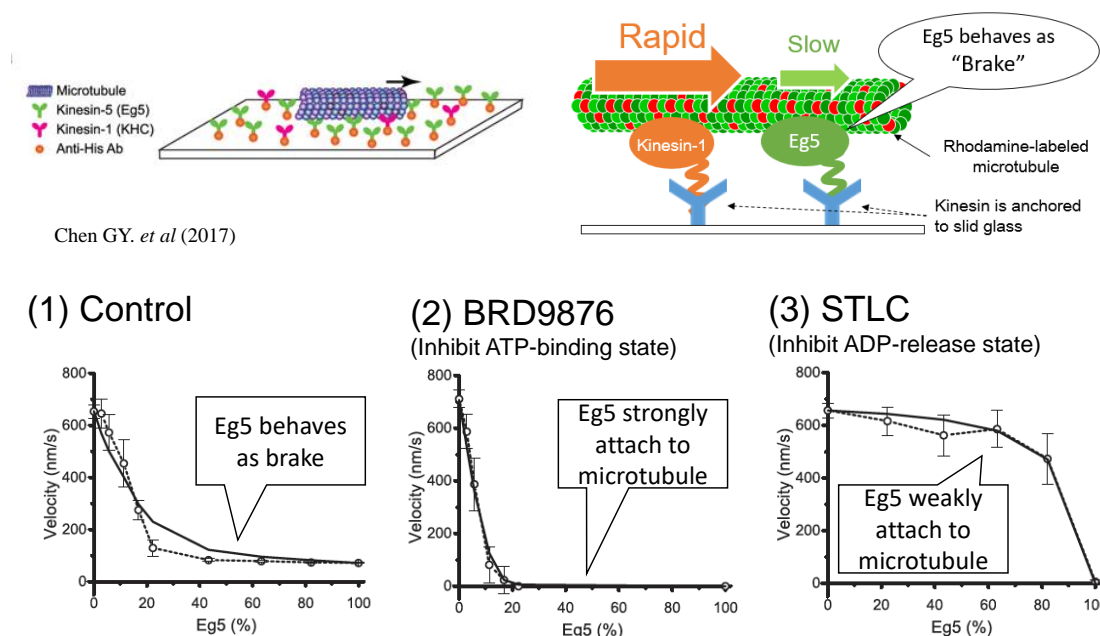
Fig. 18: **Mixed-motor gliding assay reveals where inhibitor affect to the ATPase cycle.**

(Chen, G. Y., Kang, Y. J., Gayek, A. S., Youyen, W., Tüzel, E., Ohi, R., & Hancock, W. O. (2017). Eg5 inhibitors have contrasting effects on microtubule stability and metaphase spindle integrity. *ACS chemical biology*, *12*(4), 1038-1046.)

In the control experiment, both kinesins were in normal condition and did not show any significant change in their velocity (Fig.18). In the presence of BRD9876, it showed slow velocity due to inhibition of ATP-binding state where Kinesin Eg5 strongly attached to the microtubules. However, in the case of STLC, the opposite event observed due to its ADP-binding inhibition where Kinesin Eg5 detached from the microtubules.
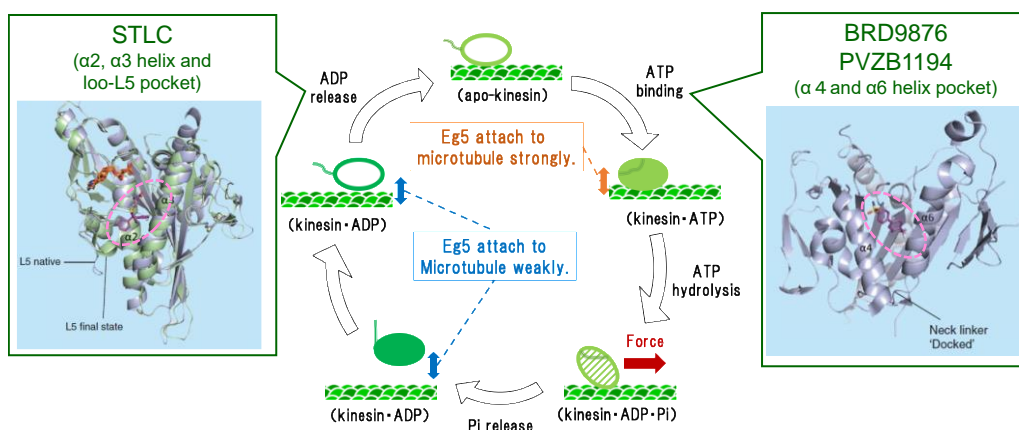
Fig. 19: Eg5 inhibitors affect to difference ATPase cycle (Chen, G. Y., Kang, Y. J., Gayek, A. S., Youyen, W., Tüzel, E., Ohi, R., & Hancock, W. O. (2017). Eg5 inhibitors have contrasting effects on microtubule stability and metaphase spindle integrity. *ACS chemical biology*, *12*(4), 1038-1046.**)**

It has been reported that Eg5 inhibitor STLC inhibits the ADP release state and another inhibitor BRD9876 inhibits the ATP binding state (Fig.19). Therefore, using this method, it is possible to clarify that the photochromic inhibitor SPSAB inhibits which state of ATPase cycles.
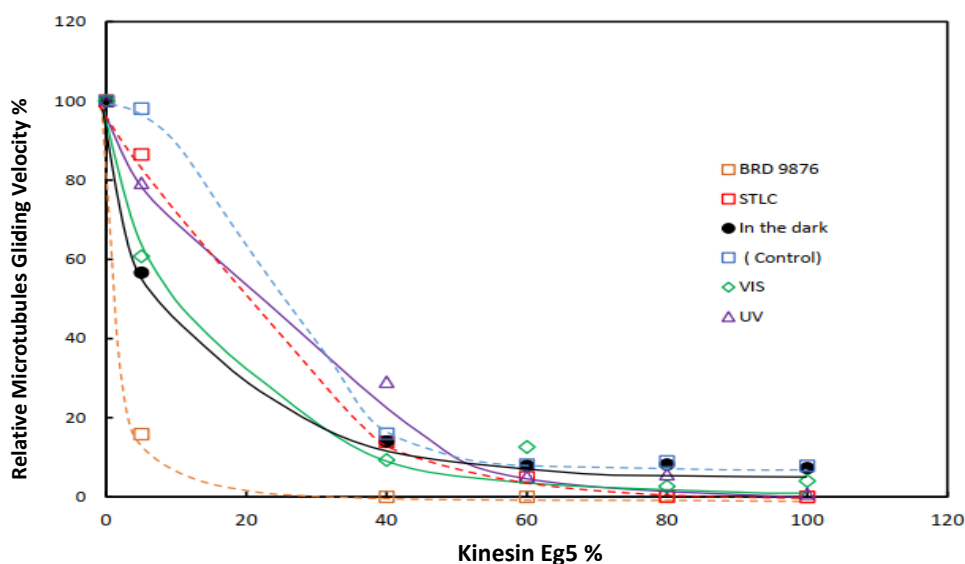
Fig. 20: Motor activity of Eg5 was evaluated by MT gliding Assay with combination of K560-CaM. The condition of the assay is - Motility buffer (10mM Tris-HCl pH 7.5, 50mM K-Acetate, 4mM MgSO4, 2.5mM EGTA), 1mM beta-mercaptoethanol and 20 µM Taxol. SPSAB 100 µM (VIS & UV) irradiated for 10 mins. In the dark – irradiated for over 24 hrs. 0.6µM conc. of Eg5 and K560-CaM, Negative Control (DMF), positive control BRD, STLC (100µM) , Rhodamine - tubulin(5mg/ml), MAPS-Free tubulin (4mg/ml).

The method of mixed motor assay has already been explained in the methods and materials part of this thesis. In this assay, two types of control were used such as- negative control DMF and positive control BRD 9876 and STLC. The result demonstrated that SPSAB inhibited Eg5 ATPase at ADP state in an ATPase kinetic pathway like STLC as shown in Fig. 20.

Discussion

The aim of this study was to develop novel photochromic kinesin Eg5 inhibitors using photochromic compounds that form three isomerization states photo-reversibly to control Eg5 function precisely, *i.e.* in a strong, medium, and weak way. Such a functionally controlled Eg5 might be applicable to cancer therapy due to its controlled medicinal effect on the patient's condition (Fig.8). The mitotic kinesin Eg5 is the target for cancer therapy and has been the focus of research because specific potent inhibitors have been found for Eg5. Interestingly, although the structures of the inhibitors are not well conserved, the inhibitors share the same binding pocket composed of loop L5, helix α2, and helix α3 near the nucleotide binding site (*15*). The only common structural characteristic among the typical potent Eg5 inhibitors is that the inhibitors contain aromatic rings linked by rotatable single bonds with localized polar functional groups. The information brought about the idea of creating novel photoresponsive inhibitors composed of photochromic molecules. Generally, photochromic compounds are composed of complex aromatic rings (*17*). In fact, some of the photochromic molecules are structurally like typical Eg5 inhibitors. For example, the partial structure of spiropyran resembles ispinesib, which is a potent inhibitor of Eg5. Therefore, it is expected that the photochromic compounds, one of isomers of which mimic the Eg5 inhibitor more effectively than the other one, may exhibit a photo-reversible inhibitory effect on Eg5.

Previously, in our laboratory, we have successfully demonstrated that the azobenzene and spiropyran derivatives exhibit photo-reversible two state inhibitory activities on Eg5 ATPase and microtubule gliding. We designed and synthesized a photochromic Eg5 inhibitor, ACTAB, composed of azobenzene, which mimics the well-known potent inhibitor STLC. ACTAB had azobenzene inserted into the position between the triethyl group and the cysteine of STLC. ACTAB showed different inhibitory activities correlating to its cis-trans as a photo-

isomerization. Therefore, the azobenzene derivative that mimics the potent Eg5 inhibitor has been shown as a photoswitch to control kinesin Eg5. However, the difference in the inhibitory activities between the two cis and trans isomerization states of ACTAB was not significant (*23*). Subsequently, photochromic inhibitors composed of two spiropyrans or two azobenzenes, were synthesized to achieve highly efficient photo switching due to the drastic structural changes induced by the double isomerizations. As expected, 2,3-bis[2,5-dioxo-{4-[(E)-2-phenyldiazen-1-yl] phenyl}pyrrolidine-3-yl)sulfanyl]butanedioic acid (BDPSB), which is composed of two azobenzenes, exhibited highly efficient photo-switching, and showed "switch ON and OFF" behavior with VIS and UV light irradiation (*24,25*)

However, the photochromic inhibitors exhibited two state inhibition, *i.e.* strong and weak switches. To achieve more multiple states, I utilized the method of coupling two different photochromic compounds together to synthesize a photochromic inhibitor. The hetero combination of photochromic molecules enables the formation of >2 isomerization states. General photochromic molecules exhibit isomerization between two different states. Coupling the different photochromic molecules theoretically generates four different isomerization states. There are various types of photochromic compounds applicable to photochromic inhibitors. For instance, Fulgide and Diarylethene, exhibit open and close ring isomerization depending on the light irradiation. Spiropyran isomerizes between the highly polar open ring zwitterion of the merocyanine isomer and the hydrophobic closed ring of the spiro isomer. Azobenzene changes its shape drastically by well-known cis and trans isomerization (*17*). The appropriate combinations selected from the photochromic molecules and their specific chemical modification might provide the photochromic Eg5 inhibitor, which exhibits effective multiple step photoswitching. However, the size and the characteristic properties of molecules composed of photochromic molecules to fit as Eg5 inhibitors are restricted.

In this study, I employed a combination of spiropyran and azobenzene to synthesize a heterodimer Eg5 inhibitor based on our previous studies on the Eg5 inhibitor composed of a homo dimer of spiropyran or azobenzene *(24,25)*. The synthesized SPSAB with the combination of spiropyran and azobenzene derivatives carries sulfonate groups at the azobenzene to increase the solubility of SPSAB. Although four isomerization states of SPSAB (SP-trans, SP-cis, MC-trans and MC-cis) are theoretically possible, I observed isomerization among the three isomers- SP-trans, MC-trans and MC-cis states but not the SP-cis state (Fig. 13). Visible light (VIS) and UV light irradiation induce SP-trans and MC-cis isomers, respectively. In the dark, azobenzene exhibits thermo dependent cis to trans isomerization, and spiropyran showed reverse photochromism in the SP state to the MC state in the aqueous buffer solution, resulting in the MC-trans state. Therefore, at this stage, it is impossible to generate the SP-cis state through light and thermal stimulations. If azobenzene and spiropyran derivatives are developed with specific and different wavelengths in the VIS range to exhibit "cis to trans" or "MC to SP" respectively, it would be possible to generate the SP-cis state.

The three isomerization states of SPSAB successfully exhibited different inhibitory activities (Fig.15 and 16). The inhibitory activity of SPSAB of SP-trans isomer for the basal and MT dependent ATPase activity of Eg5 exhibited potent IC_{50} values, whereas MC-trans and MC-cis exhibited medium and weakly IC_{50} values.

However, among the three isomerization reactions of SPSAB, it is notable that the value of V_{max} was not influenced, whereas it decreased the affinity of Eg5 for MTs in MT-dependent ATPase (Fig. 16). Hence, all the isomerization reactions of SPSAB might have an allosteric binding site on Eg5, where the MT binding site was affected. In the presence of SP- trans, a sigmoidal curve was observed in MT-dependent ATPase of Eg5. This indicates the presence of allosteric binding sites of Eg5 such as MT-binding regions α4 and α6.

Moreover, in the presence of the SP-trans isomer, the MT gliding velocity was significantly reduced due to the dissociation of MTs from Eg5, as shown in the *in vitro* motility assay (Fig. 17). On the other hand, in the MC- trans and MC-cis isomers, the dissociation of MTs was not prominent and reduced the velocity as mediumly and weakly. In Fig. 20, the mixed motor motility assay result demonstrated that the inhibitory behaviors of SPSAB are similar to well-known Eg5 inhibitor STLC. Therefore, this study proved that the photochromic molecules are valid as a photo-switching device to control the inhibitory activity of the mitotic kinesin Eg5 inhibitor.

Conclusion

I have shown that the novel photo-responsive kinesin Eg5 inhibitor, SPSAB, forms three isomerization states, SP-trans (VIS), MC-cis (UV), and MC- trans (in the dark). The photochromic inhibitor SPSAB significantly affected the activity of Eg5. Most importantly, the formation of three states was achieved to control Eg5 precisely. It is expected that the three states of SPSAB may provide more options for the treatment of cancer.

Chapter 3

Kolaflavanone, a biflavonoid derived from medicinal plant Garcinia, is an inhibitor of mitotic kinesin Eg5

Introduction

Kinesin Eg5 is a homotetrameric motor protein that moves towards the plus-end of microtubules in cells and plays essential roles in cell division through the formation of mitotic spindles and maintenance of spindle bipolarity (*28–33*). In dividing cells, replicated cellular materials (DNA) are usually separated into new (daughter) cells by a complex process involving the mitotic spindles. Selective inhibition of Eg5 disturbs the formation of functional spindles and normal chromosomal separation with a concomitant formation of monopolar spindles in tumor cells, causing mitotic cell arrest or apoptosis (*34–39*). Therefore, Eg5 has been recognized as an important target for antimitotic agents in cancer treatment. An advantage of targeting Eg5 lies in the peculiar structural characteristics of the protein—an elongated loop5—that enhances the selectivity and affinity of its inhibitors. In addition, the protein is reportedly absent in the adult human central nervous system, which indicates that inhibition of Eg5 may not lead to neurotoxicity (*40,41*).

Eg5 inhibitors have been identified from both natural and synthetic sources which shown in several studies. Monastrol, S-trityl-L-cysteine (STLC), and ispinesib are some examples of synthetic small molecule inhibitors of the Eg5 (*36, 42, 43*). Nevertheless, the natural sources of Eg5 inhibitors remain relatively less explored. Only a few natural Eg5 inhibitors are known with therapeutic benefits and biologically active compounds, such as gossypol, terpendol E, and adociasulfate-2 (*36, 44, 45*). Medicinal plants are an essential component of natural remedies, which are constantly being researched for their positive medicinal value and biologically active compounds. Garcinia species are well-known for their strong biological activity in a variety of experimental fields. As the primary phenolic component, a yellowish extract known as kolaviron was extracted from the nuts of Garcinia kola (*46*). A wide range of pharmacological activities, including antioxidant, hypoglycemic,

48

radio-protective, anti-inflammatory, hypolipidemic, antibacterial, hepatoprotective, analgesic, gastroprotective, neuroprotective, and anticancer effects have been reported for kolaviron over the years (*47–52*).

The active chemicals in kolaviron, Garcinia biflavonoid (GB) 1, GB 2, and kolaflavanone (KLF), have been discovered as bioflavonoids. This is not surprising, as most biflavonoids are physiologically active and show higher therapeutic efficacy than their corresponding monoflavonoids (*53*). Anticancer action has been observed in biflavonoids from a variety of plants, although the molecular targets and underlying mechanisms for this effect have remained poorly studied (*54–56*). Notably, Kolaviron showed anti-proliferative and anti-angiogenic properties *in vivo*, along with favorable benefits in the treatment of benign prostatic hyperplasia (*57,58*).

Morelloflavone, another biflavonoid analogue, has already been shown to inhibit Eg5 (*59*). KLF is a biflavonoid having a structural resemblance to morelloflavone. As a result, it may also inhibit the ATPase function of Eg5. Reports have shown the inhibitory effect of KLF against tyrosinase (*60*), as its interaction with serum albumin and aldehyde dehydrogenase, a key enzyme in detoxification processes (*61, 62*). However, the biochemical analysis of KLF interaction with Eg5 has not been performed. As a result, I investigated the influence of KLF on Eg5 ATPase and motility activities. The data presented in this study demonstrate the allosteric inhibition of Eg5 ATPase and microtubule-gliding activity of Eg5-KLF interaction.

Materials and methods

In vitro experimental procedure

Chemicals

KLF was kindly provided by Dr. Kolawole of the Federal University of Technology, Akure, Nigeria (*62, 63*). All other chemicals used in the study were of analytical grade.

Kinesin Eg5

Recombinant Eg5 was prepared as previously described (*64*). Briefly, cDNA of mouse Eg5 motor domain (wild type [WT], residues 1-367) was amplified by polymerase chain reaction (PCR) and ligated into the pET21a vector. The WT Eg5 expression plasmids were used to transform *Escherichia coli* BL21 (DE3) cells. Eg5 WT was then purified with a Co-nitrilotriacetic acid column, which was washed with lysis buffer containing 30 mM imidazole. Bound Eg5 was eluted with lysis buffer containing 150 mM imidazole. The obtained fractions were analyzed by sodium dodecyl sulfate-polyacrylamide gel electrophoresis (SDS-PAGE), whereas dialysis of purified Eg5 was performed using a buffer containing 30 mM Tris-HCl (pH 7.5), 120 mM NaCl, 2 mM $MgCl_2$, 0.1 mM ATP, and 0.5 mM DTT. Finally, the purified Eg5 was stored at -80°C until further use.

Tubulin purification and polymerization

The tubulin used in this study was purified from the porcine brain as originally described by Hackney (*65*) and stored at -80°C until further use. Tubulin was polymerized at 37°C for 30 min using a buffer containing 100 mM Piperazine-1,4-bis(2-ethanesulfonic acid) (PIPES; pH 6.8), 1 mM *O,O'*-bis(2-aminoethyl)ethyleneglycol- *N,N,N',N'*-tetraacetic acid (EGTA), 1 mM $MgCl_2$, and 1 mM GTP. Taxol was added at a final concentration of 10 mM.

Polymerized microtubules were then collected after centrifugation at 280,000 × g for 15 min at 37°C. After discarding the supernatant, the microtubule pellet was dissolved in a buffer containing 100 mM PIPES (pH 6.8), 1 mM EGTA, 1 mM MgCl$_2$, 1 mM GTP, and 10 mM taxol.

ATPase assay

ATPase activity was measured at 25°C in an ATPase assay solution (20 mM HEPES-KOH [pH 7.2] containing 50 mM KCl, 2 mM MgCl$_2$, 0.1 mM EGTA, 0.1 mM EDTA, and 1.0 mM β-mercaptoethanol) using 0.5 μM Eg5 (for basal ATPase activity) or 0.1 μM Eg5 (for microtubule-activated ATPase activity). To measure the inhibitory activity, Eg5 was pre-incubated for 5 min and 20 min in the presence and absence of 3.0 μM microtubules, respectively, and supplemented with 0–250 μM KLF dissolved in DMF. ATPase activity was initiated by adding 2.0 mM ATP, terminated after 5 (MT-activated ATPase) and 20 min (basal ATPase) by adding 10% trichloroacetic acid (TCA), and estimated based on inorganic phosphate (Pi) released into the supernatant, as quantified by the Youngburg method (*66*), as described by Ogunwa *et al.* (*60*). To assess the effects of KLF on microtubule-dependent activity, ATPase turnover was also measured in the presence of 100 μM KLF and 0–12 μM microtubules.

Microtubule-gliding assay

The motor activity of kinesin Eg5 was investigated by performing a microtubule gliding experiment (*64, 67*). For the microtubule-gliding assay, rhodamine-labeled tubulin was prepared and mixed with unlabeled tubulin at a ratio of 1:5 and left to polymerize for 40 min at 37°C in a buffer solution containing 100 mM PIPES, 2 mM EGTA, and 1 mM MgSO4. Taxol was then added at a final concentration of 20 μM. Next, coverslips were coated with anti-6x histidine monoclonal antibody (Wako) in an assay solution containing 10 mM Tris-acetate (pH

7.5), 2.5 mM EGTA, 50 mM K-acetate, and 4mM $MgSO_4$. Then, the flow chambers were flushed with 0.1 µM Eg5 in assay solution A (10 mM Tris-acetate [pH 7.5], 4 mM $MgSO_4$, 50 mM potassium acetate, 2.5 mM EGTA, 0.5 mg/mL casein, and 0.2% β-mercaptoethanol) and incubated for 5 min at 25°C. The chamber was then washed with rhodamine-labeled microtubules in assay solution B (20 mM taxol added to assay solution A) and incubated for 2 min. Subsequently, assay solution B was flushed through the chambers, followed by 150 µM KLF and 1.0 mM ATP in assay solution C (assay solution B, 1.5 mg/mL glucose, 0.05 mg/mL glucose oxidase, and 0.01 mg/mL catalase). Lastly, rhodamine-labeled microtubules were visualized using an Olympus BX50 microscope equipped with a charge-coupled device (CCD) camera (LK-TU53H, Toshiba, Japan).

In silico modeling

Protein preparation

The starting coordinates for Eg5 were retrieved from the RSCB Protein Data Bank (http://www.rcsb.org/pdb, PDB ID: 3KEN), which correspond to Eg5 with ADP and STLC bound to the nucleotide-binding and allosteric sites, respectively. Ligands and crystallographic water molecules outside these binding sites were deleted before molecular docking studies.

Ligand selection, preparation, and optimization

The 2D chemical structure of KLF was obtained from the report of Kolawole *et al.* (*62*), and the 3D structure was retrieved from the NCBI PubChem compound database (http://www.ncbi.nlm.nih.gov/pccompound).

Molecular docking

Ligand docking and binding site analyses were performed using the AutoDock Vina suite in PyMol (*68, 69*). In brief, blind docking was performed with grid parameters x = 200, y = 200, and z = 200 to ensure that all available binding pockets in Eg5 are accessible to KLF, with sufficient room for full ligand rotation and translation. The spacing between the grid points was maintained at 0.375 Å. While the rotatable bonds in the ligand were not restrained, the protein molecule was treated as a rigid structure. Multiple docking runs were performed for each ligand with the number of modes set to 10 to achieve more accurate and reliable results. The binding energies were estimated for the best fit.

Molecular dynamics simulation

The Eg5-KLF complex obtained from molecular docking with the best fit was subjected to atomistic simulation experiments using Groningen Machine for Chemical Simulations (GROMACS) version 5.0, with an AMBER99SB-ILDN force field (*70, 71*). As control experiments, apo Eg5 (without any ligand), Eg5-ADP, and Eg5-ATP complexes were also subjected to atomistic simulations. First, the ligands were parameterized using the AnteChamber PYthon Parser interfacE (ACPYPE). The protein-ligand biosystems were then prepared using the parameters in the gro files of both protein and ligands, which were merged and placed at the center of a box at a distance of 2.0 nm away from the box wall in all directions. Solvation of the biosystems with a transferable intramolecular potential three-point (TIP3P) water model was performed, followed by neutralization using Na^+/Cl^- ions (0.15 M). Minimization was performed using the steep-descent algorithm (50,000 steps). Equilibration was performed using a leapfrog integrator for equations of atomic motion with time-steps of 2 fs at a constant number of particles, volume, and temperature (NVT) and 1 ns at a constant number of particles, pressure, and temperature (NPT) conditions. The temperature was

maintained at 300 K using the Berendsen thermostat algorithm, and the Parrinello-Rahman barostat algorithm was used to maintain the pressure at 1 bar. During these steps, protein and ligand, as water and ions, were coupled to their temperature and pressure, while a full positional constraint was imposed on the heavy atoms in all directions using the linear constraint solver (LINCS) algorithm for bond constraint (*72*). The particle-mesh Ewald (PME) summation scheme was used to estimate the long-range electrostatic interactions, and each cut-off distance was maintained by the Verlet scheme. The van der Waals interactions were monitored at 10 Å. Based on evidence from the literature (*73*), unrestrained production phase simulation for 100 ns was performed on each of the biosystems at pH 7.0.

Data analysis

ATPase activity was plotted against the KLF concentration to obtain IC_{50} values. Data from biochemical experiments are reported as the mean ± standard deviation (SD). Significant differences between groups were tested using Welch's *t*-test or Student's *t*-test. Protein-ligand complexes and molecular interactions were created using PyMol. GROMACS *in-built* analysis tools (*g_rmsd*, *g_Rg*, and *g_dist*) were used. The MD trajectory was visualized using visual molecular dynamics (VMD). Similarly, the water density was calculated using the Volmap plugin in VMD.

Results and Discussion

KLF inhibits Eg5 ATPase activity

Fig. 21 shows the chemical structure of KLF, a biflavonoid constituent of kolaviron. The compound is comprised of apigenin and 4-methyl-quercetin. To ascertain the potential of KLF to interact with kinesin Eg5 and inhibit its function, the basal ATPase activity was measured in the absence of microtubules at various concentrations (0–250 µM) of KLF.
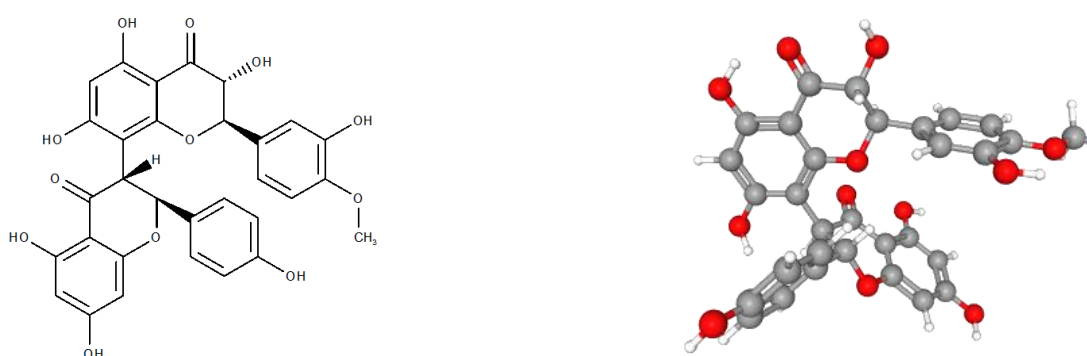
Fig. 21: Chemical structure (2D and 3D) of kolaflavanone (KLF).

As shown in Fig. 22A, KLF inhibited the basal ATPase function of Eg5 in a dose-dependent manner with an IC_{50} value of 98 µM. Next, I evaluated the effect of KLF on the microtubule-activated ATPase activity of Eg5. The results revealed a concentration-dependent inhibition with an IC_{50} value of 125 µM (Fig. 22B). The inhibitory activity of KLF on the basal ATPase activity of Eg5 was more potent than that of microtubule-activated activity, indicating that microtubules moderate the inhibitory potency of KLF. The difference in the IC_{50} of basal and microtubule-activated ATPase activities is compatible with that reported for monastrol, the first Eg5 inhibitor discovered (74). Relative to known Eg5 inhibitors derived from natural products, KLF displayed a higher IC_{50} value.
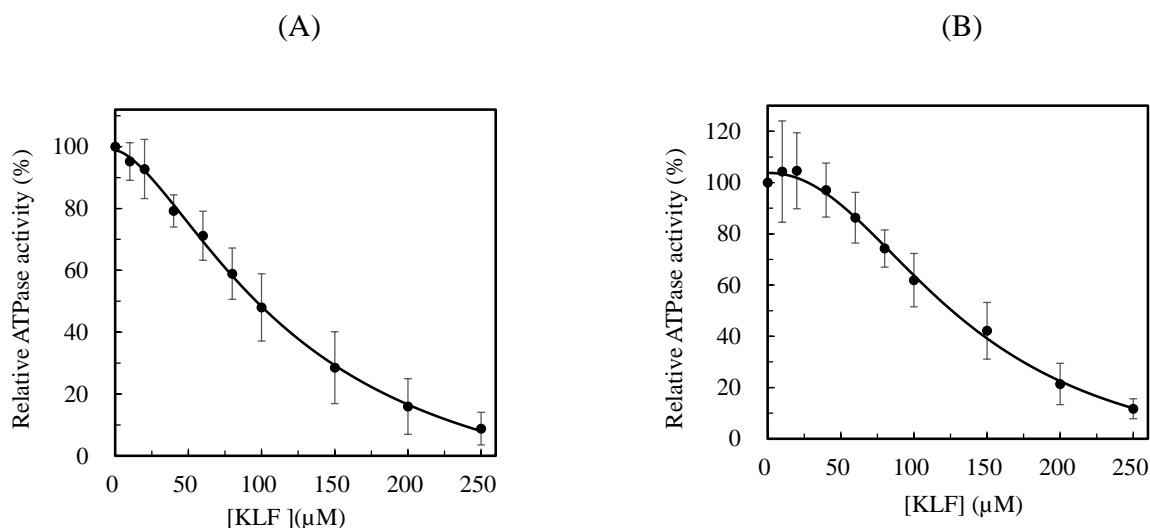
Fig. 22: Effect of kolaflavanone (KLF) on the *in vitro* ATPase activity of Eg5. **(A)** Basal Eg5 ATPase activity measured in 20 mM HEPES-KOH (pH 7.2), containing 50 mM KCl, 2 mM $MgCl_2$, 0.1 mM EGTA, 0.1 mM EDTA, 1.0 mM β-mercaptoethanol, and 0.5 μM Eg5. The reaction was initiated by adding 2.0 mM ATP, and ATPase activity was measured for 20 min at 25℃ in the presence of 0–250 μM KLF. Data were collected from three independent experiments. **(B)** Microtubule-activated Eg5 ATPase activity was measured for 5 min at 25℃ in the presence of 3.0 μM microtubules, 0.1 μM Eg5, and 0–250 μM KLF.

This suggests that the potency of KLF is lower than that of inhibitors like terpendole E (IC_{50} 23 μM, *45*), gossypol (IC_{50} 10.8 μM, *44*), and adociasulfate-2 (IC_{50} 3.5 μM, *46*) but like that of morelloflavone (IC_{50} 98 μM, *60*). The basal ATPase IC_{50} value of morelloflavone was higher than that of microtubule activated IC_{50}. Conversely, KLF displayed a lower IC_{50} value for basal than microtubule activated IC_{50} in the ATPase assay (*60*).

KLF suppresses motor gliding of Eg5 on microtubules

Further, I investigated the effect of KLF on Eg5 gliding along fluorescently labeled microtubules. Eg5 motor activity on microtubules was suppressed within 900s at varying concentrations of KLF (0–150 μM) (Fig. 23A). The gliding velocity of Eg5 was reduced to 4.20 ± 1.00 nm/s in the presence of 100 μM KLF relative to that recorded for the control (9.02 ± 1.4 nm/s) in the absence of KLF. The velocity of Eg5 was further reduced to 3.7 ± 1.0 nm/s when KLF concentration was increased to 150 μM. These observations suggest the potential of KLF in blocking the movement of Eg5 along microtubules, and the results are consistent with previous reports indicating the ability of inhibitors to block Eg5 motor function (*75, 76*).
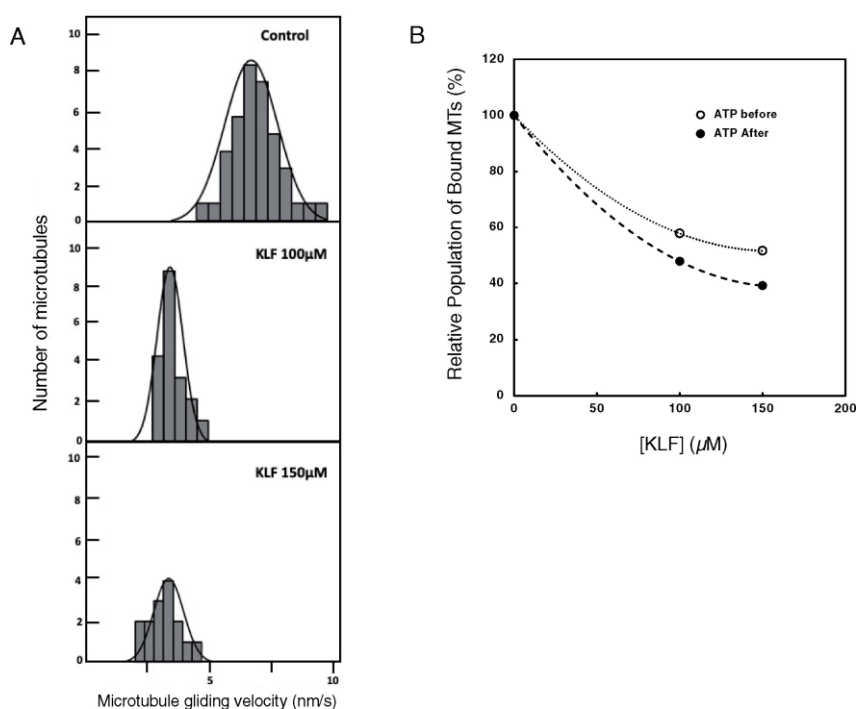
Fig. 23: Effect of kolaflavanone (KLF) on the motility of Eg5. **(A)** Effect of KLF on Eg5 motor function in the absence of KLF and the presence of 100 and 150 μM KLF. **(B)** Determination of the number of microtubules before and after applying ATP in the flow cell. Data were collected from three independent experiments. The motility of Eg5 was measured in a solution containing 10 mM Tris-HCl (pH 7.5), 50 mM potassium acetate, 4 mM $MgCl_2$, 2.5 mM EGTA, 1.0 mM β-mercaptoethanol, 20 μM taxol, 0.15 μM rhodamine-labeled microtubules, and 0.6 μM Eg5. The movement of

rhodamine-labeled microtubules was initiated by adding 1.0 mM ATP and was observed for 900 s at 25°C using fluorescence microscopy.

Compared to morelloflavone, our results suggest a 3-fold motility suppression of Eg5 at 100 µM KLF. At 150 µM KLF, the Eg5 velocity was suppressed by 41%. However, morelloflavone suppressed Eg5 velocity by 47.2 % at a higher concentration of 250 µM (*60*). I observed that the suppression of Eg5 velocity by KLF was associated with a decrease in the number of microtubules (Fig. 23B). By increasing the concentration of KLF, it appears that the biflavonoid induces dissociation of microtubules from Eg5. To confirm this observation, I determined the number of microtubules before and after ATP application in the flow cell. The results suggested that KLF induces microtubule dissociation, as shown in Fig. 23B.

Interaction mechanism between kinesin Eg5 and KLF

To gain more insights into the interaction between KLF and Eg5, including the possible binding site on the motor domain of Eg5, I investigated whether KLF competes with ATP at the nucleotide-binding pocket. The concentration of ATP was increased from 0 to 250 µM in the absence of microtubules, whereas the concentration of KLF was fixed at 100 µM, which was chosen based on its IC_{50} in the basal ATPase activity. As shown in Fig. 24A, KLF does not directly compete with ATP binding at the nucleotide-binding (active) site. The V_{max} for ATP was reduced from 3.37 ± 0.37 s^{-1} in the absence of KLF to 2.47 ± 0.55 s^{-1} in the presence of 100 µM KLF. However, the K_m for ATP (35.77 µM) in the absence of KLF was very similar to that at 100 µM KLF (35.23 µM). Indeed, the K_m of ATP obtained for Eg5 in this study is compatible with that reported by Cochran *et al.* (*43, 70*) and Lad *et al.* (*42*). These data suggest that KLF inhibits Eg5 via a noncompetitive mechanism rather than a competitive mechanism in which an inhibitor is expected to increase K_m without altering the V_{max} (*73, 76*). Similarly, I evaluated the ATPase activity of Eg5 in the presence of 100 µM KLF while varying the

microtubule concentration from 0 to 12 µM (Fig. 24B). The K_{MT} obtained for microtubule association of Eg5 in the absence of KLF was 0.98 µM, and the V_{max} was 31.55 s^{-1}. However, the value of K_{MT} was increased to 2 µM in the presence of 100 µM KLF, whereas that of V_{max} was decreased to 28.38 s^{-1}.
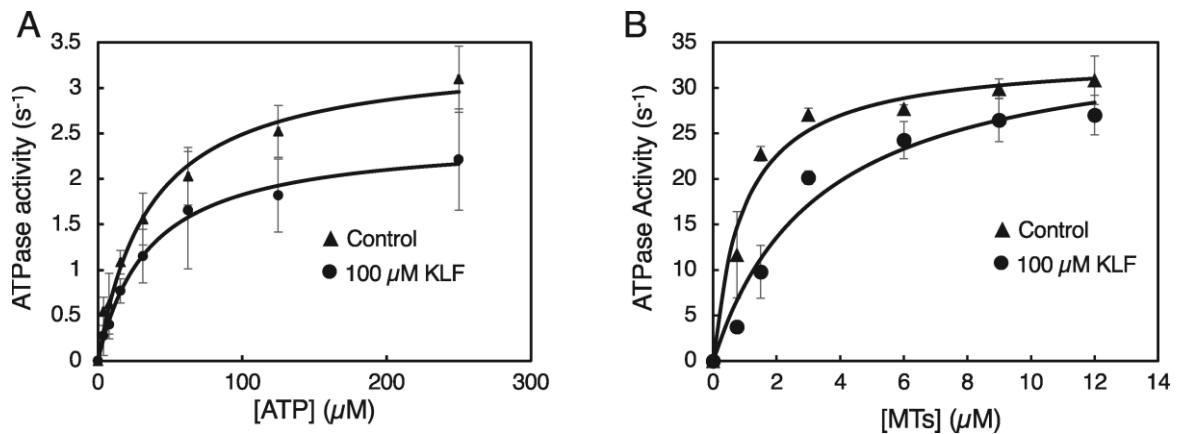
Fig. 24: Effect of kolaflavanone (KLF) on the MT-dependent Eg5 ATPase activity. (A) The ATPase activity of 0.1 µM Eg5 in the presence of 0.5 µM microtubule and 0 µM (triangle) and 100 µM (circle) KLF. Data were collected from three independent experiments. **(B)** ATPase assay with 0–12 µM microtubules and 100 µM KLF.

Since both K_{MT} and V_{max} for microtubule binding were altered, these results indicate that the affinity of Eg5 for microtubules was modulated by the presence of KLF, and the inhibitor did not compete with microtubule binding. The interaction of KLF with the allosteric pocket of Eg5 might stabilize the bound nucleotide (ADP) and induce the formation of a weak-binding state, resulting in inhibition of basal and microtubule-stimulated ATPase activity (*42*).

Specificity of inhibitory effect of KLF against kinesin Eg5

The inhibitory effect of KLF was mapped out on conventional kinesin (kinesin 1) to evaluate whether the inhibitory effect of KLF is specific to Eg5 among the kinesin superfamily. As shown in Fig. 25, KLF suppressed the microtubule-activated ATPase activity of kinesin-1 (22%) and Eg5 (62%) at 150µM. The effect was dose-dependent, suggesting that the inhibition may be caused by the binding of KLF to a similar site on both Eg5 and conventional kinesin. However, the affinity of KLF for kinesin-1 was lower than that for Eg5. Previous crystallographic and computational studies of Eg5 and kinesin-1 have shown that the loop5 is more elongated in Eg5 than in conventional kinesin (*79–82*). Since this loop contributes to the formation of the allosteric binding pocket of Eg5, it may explain the weaker binding affinity of KLF for kinesin 1.
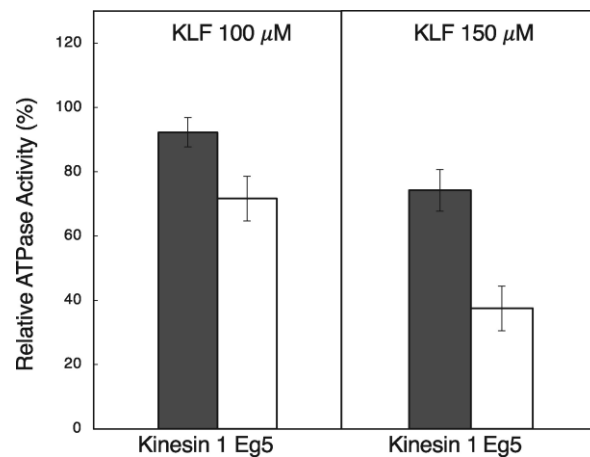
Fig. 25: Inhibitory effect of kolaflavanone (KLF) on the ATPase activity of conventional kinesin versus Eg5. The microtubule-activated ATPase activity of conventional kinesin (kinesin-1) was measured in the presence of various concentrations of KLF and compared with Eg5. The ATPase activities of 0.1 µM motor domain truncated kinesin-1 (1–560 amino acids) or Eg5 were measured in a solution of 20 mM HEPES-KOH (pH 7.2) containing 50 mM KCl, 2 mM $MgCl_2$, 0.1 mM EDTA, 0.1 mM EGTA, 1.0 mM β-mercaptoethanol, 2.0 mM ATP, 3.0 µM microtubule, and 0-150 µM KLF at

25^0C. Data are representative of three independent experiments and are expressed as the mean ± standard deviation.

Atomistic basis of Eg5-KLF interaction

The results from the kinetics studies suggest that KLF inhibits Eg5 through an allosteric mechanism (Fig. 24). To model the plausible binding pattern of KLF on the allosteric pocket of Eg5, a molecular docking experiment using a blind docking approach was performed to allow KLF to identify its most preferred binding site. Visual observation of Eg5-KLF complex generated from the experiment in PyMol revealed that KLF is stably bound to the putative L5/α2/α3 pocket (L5: Gly117-Gly134, α2: Lys111-Glu116 and Ile135-Asp149, α3: Asn206-Thr226) similarly to monastrol, the first known inhibitor of Eg5 (Fig. 26A and B). This validates the allosteric mechanism of KLF, which is positively correlated with the data from wet experiments. The L5/α2/α3 allosteric pocket accommodates known inhibitors of Eg5 with diverse chemical scaffolds, size, and potency (*81*). Interestingly, Eg5 inhibitors that bind the L5/α2/α3 pocket is the most investigated because of their selectivity and affinity, as conferred by the elongated loop5 (L5).
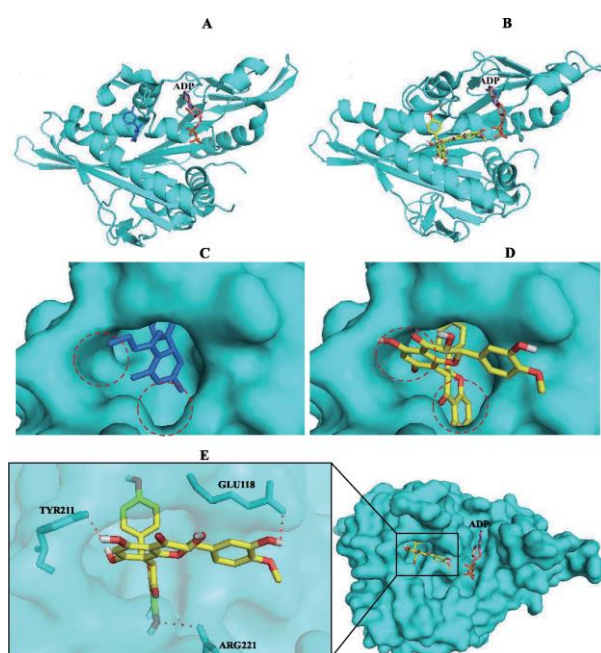
Fig. 26: *In silico* modeling of Eg5-kolaflavanone (KLF) interaction. (A) Binding of known Eg5 inhibitor (monastrol) to Eg5. **(B)** Binding of KLF to Eg5. Comparison of binding pattern of **(C)** monastrol and **(D)** KLF. **(E)** Interacting residues of Eg5 with KLF at the allosteric pocket.

These inhibitors act via a similar mechanism, involving the induction of conformational changes in Eg5 to suppress ADP release (*42, 43*). Comparing the binding mode of KLF with monastrol, it was observed that both compounds bind to the same pocket on Eg5 (Fig. 26C). However, the KLF moieties completely occupied the allosteric pocket compared to monastrol (Fig. 26D). In particular, the so-called "co-operative binding pocket" on the Eg5 allosteric site was occupied by aromatic rings of KLF, such as STLC and Ispinesib (*82–84*). However, the lower potency of KLF compared to the synthetic inhibitors suggest that the degree of conformational changes induced at the nucleotide-binding site and other important regions such as the microtubule-binding site may underlie the differences in the degree of inhibition rather than the binding pattern alone (*42, 73, 83, 84*). In addition, the chemical moieties such as the sulfanylidene, dihydro-1H-pyrimidine and carboxylate moieties present in monastrol may contribute to its higher potency. A detailed observation within 4 Å of KLF in the allosteric pocket revealed three hydrogen bonds formed by the hydroxyl groups of Glu118, Tyr211, and Arg221 (Fig. 26E). Specifically, the amine group of Arg221, the phenolic portion of Tyr211, and the carboxylic moiety of the Glu118 side chain are involved in the hydrophilic interaction. These amino acid residues have been reported to stabilize inhibitors in the L5/α2/α3 pocket via hydrogen bond formation (*83–85*).

Molecular dynamics studies of Eg5-KLF complex

To further evaluate the stability of Eg5-KLF complexes in the presence of nucleotides (ATP and ADP), molecular dynamics simulations (MDS) were performed. I modeled five Eg5 complexes: Apo-Eg5, Eg5-ADP, Eg5-ATP, Eg5-ADP-KLF, and Eg5-ATP-KLF. The crystal structure of Eg5 (PDB ID: 3HQD) was adopted as the initial Eg5 coordinates corresponding to Eg5-ATP complex whereas crystal with PDB ID: 1II6 was used for the Eg5-ADP complex. All missing residues were modeled before the simulations. To generate the Eg5 apo state, the ADP of crystal structure (PDB ID: 1II6) was simply deleted. The Eg5-nucleotide-KLF complexes used for simulation were generated from the molecular docking experiment. Each biosystem was subjected to a 100 ns simulation, and the data were analyzed. Visual observation of the Eg5-nucleotide-KLF complexes throughout the simulation trajectory showed that KLF was stably resident in the L5/α2/α3 allosteric pocket which is consistent with the result from molecular docking (Fig. 26B). The root means square deviation (RMSD) values of Eg5 C-α carbon suggest that the Eg5-KLF complexes in the presence of ADP or ATP were stable and converged early into the simulation (Fig. 27A). However, the apo-Eg5 complex showed the lowest stability and achieved convergence at 60 ns. In the presence of KLF, amino acid residues around the allosteric pocket exhibited rigidity, as inferred from the distance between Lys207 (K207) and Glu128 (E128). This observation correlates with the conformational changes and dynamics induced by ligand binding in the allosteric pocket (Fig. 27B). Concurrently, apo-Eg5 has the highest flexibility in the allosteric binding region, depicting the putative Eg5 behavior in the absence of ligands.
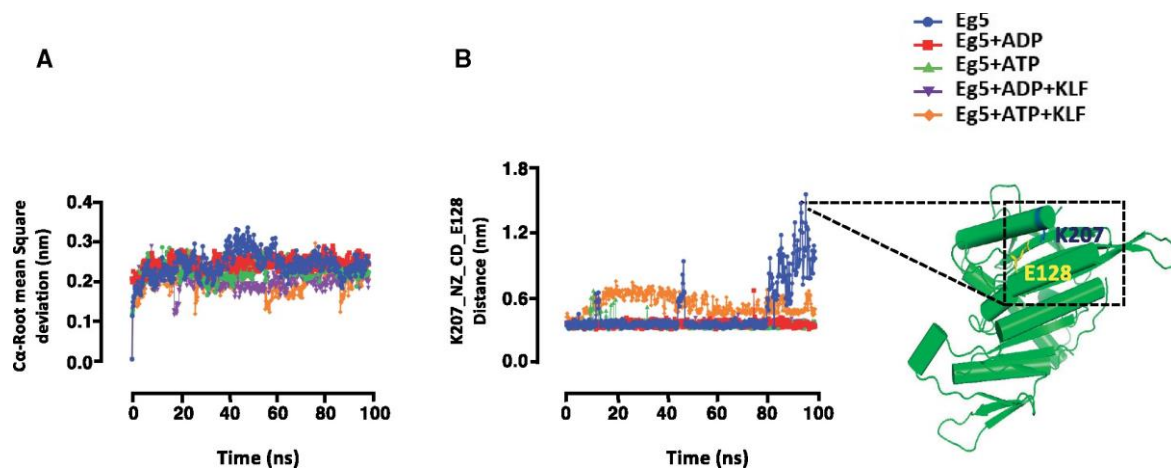
Fig. 27: Stability of Eg5-kolaflavanone (KLF) complexes in the presence of ATP and ADP.
(A) The root means square deviation (RMSD) of Eg5-KLF complexes in the presence of nucleotides. **(B)** Effect of KLF on the conformational behavior of Eg5 around the binding pocket.

Fig. 28 shows the essential dynamics of the Eg5-nucleotide structures under different ligand conditions. The Eg5 structure comprises numerous loops, α-helices, and β-sheets (Supplementary fig.1). The spatial arrangement of these unique segments (Fig. 28A) supports their peculiar role in protein structural flexibility and catalytic function. In this study, KLF binding to the allosteric pocket of Eg5 altered the essential dynamical behavior of the protein. Notably, in the apo-Eg5 complex, the loop8, loop10 and β6 regions displayed increased flexibility (Fig. 28B). However, ADP binding in the structure abolished the dynamic pattern of loop8 and loop11 while retaining the flexibility of loop10 (Fig. 28C). The Eg5-ATP complex showed a relatively rigid structure with less flexibility in the L11 region, one of the conserved structural elements of kinesin near the ATP-binding site previously shown to respond to motor domain nucleotide-state (*86*). Loop11 has been reported for its essential role in the interaction of Eg5 and microtubules at the Eg5-microtubule interface (Fig. 28D).

64
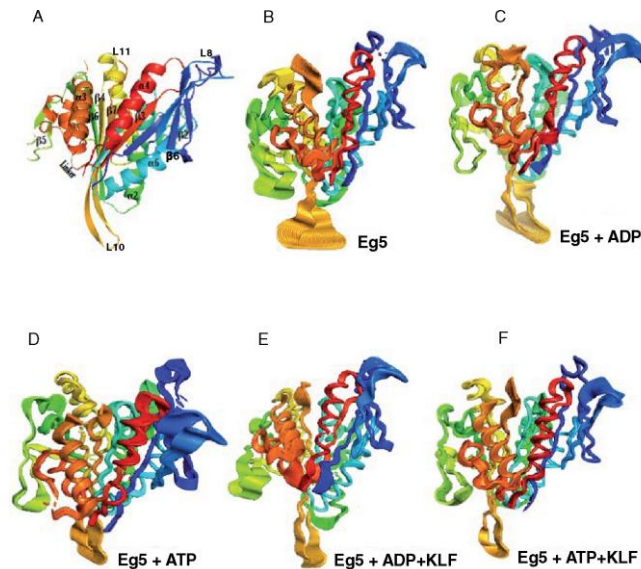
Fig. 28: Essential dynamics of Eg5 conformation in the presence and absence of kolaflavanone (KLF). (A) Eg5 structure showing the important α, β, and loop regions. **(B)** Structures of apo Eg5, **(C)** Eg5-ADP complex, **(D)** Eg5-ATP complex, **(E)** Eg5-ADP-KLF complex, and **(F)** Eg5-ATP-KLF complex.

Previous studies and available crystal structures have confirmed that the loop11/helix 4 junction is positioned in close contact with the interface of αβ-tubulin in the structures of tubulin-bound kinesin, where it extends from the motor domain and make physical contact with the tubulins (*86*). Hence, the loop11 is placed in an ideal location to detect perturbations in the αβ-tubulin heterodimer curvature as sensing the subtle changes in the conformations of tubulins (*87–89*). KLF binding to Eg5 in the ADP- or ATP-binding state altered the conformation of Eg5 loop11 compared to the apo- and nucleotide-bound states (Fig. 28E and F). This may contribute to the observed dissociation of microtubules from Eg5 in the motility assay (Fig. 23B) since an altered loop11 conformation of Eg5 at the interaction interface may result in a weak binding to microtubule. The loop10, β4, β6, and regions showed a significant reduction in their flexibility during simulation compared to apo-Eg5. These data suggest that

conformational changes occurred in Eg5, inducing KLF binding to the allosteric pocket. This may contribute to the inhibitory mechanisms of the novel inhibitor against the ATPase and motility functions of the enzyme, as a relatively rigid conformation of Eg5 may exhibit weaker binding to microtubules. Indeed, inhibitors that interact with the allosteric pocket of Eg5 are known to cause conformational changes in the protein structure, which leads to the inhibition of ATPase function with a concomitant impediment to microtubule-gliding activity. Notable adjustments have been reported in the allosteric pocket after inhibitor binding, which researchers speculate might have caused the extensive change in the enzyme conformation (*42,80,90*). I estimated the water density in both nucleotide-binding and allosteric pockets of Eg5 in the presence and absence of KLF during the simulation. Fig. 29A shows that the water molecules densely occupied the L5/α2/α3 and ATP-binding pockets during the simulation in the Eg5 apo state. However, the water density at the nucleotide-binding cleft was highly reduced in the nucleotide-bound (Eg5-ADP and Eg5-ATP) states (Fig. 29B and C).
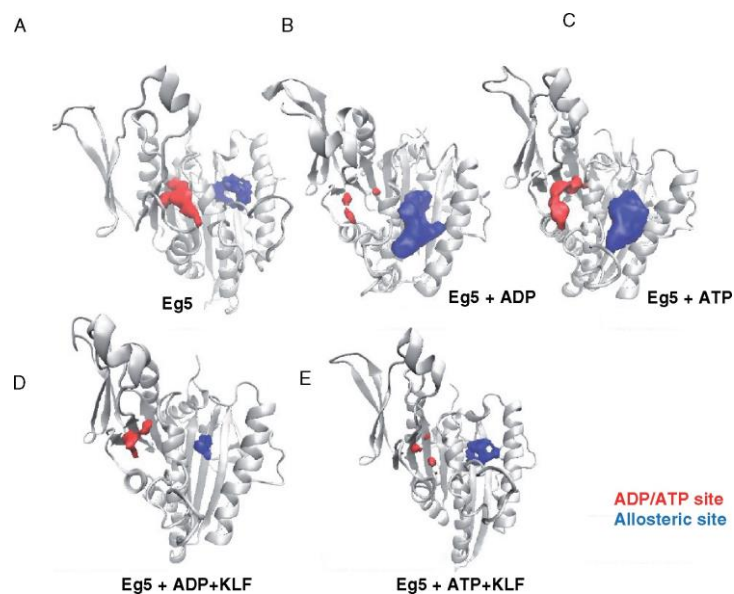
Fig. 29: Kolaflavanone (KLF) binding reduced water clustering within the allosteric L5/α2/α3 pocket (blue blobs) and nucleotide-binding site (red blobs) of Eg5 motor domain. **(A)** Structures of apo Eg5, **(B)** Eg5-ADP complex, **(C)** Eg5-ATP complex, **(D)** Eg5-ADP-KLF complex, **(E)** Eg5-ATP-KLF complex.

Interestingly, the binding of KLF to the L5/α2/α3 pocket led to a reduction in the solvation of the allosteric pocket (Fig. 29D and E), indicating that KLF resides stably in the allosteric pocket during the simulation and the associated conformational changes at the ATP-binding site. These results validate the affinity of KLF for Eg5 as an inhibitor and confirm the stability of the Eg5-KLF complexes.

Conclusion

This study investigated KLF, a biflavonoid derived from *Garcinia kola*, as a novel inhibitor of mitotic kinesin Eg5. KLF inhibited the ATPase activity of Eg5 in basal and microtubule-activated states. Furthermore, the microtubule-gliding function of Eg5 was suppressed by KLF. KLF allosterically inhibited the ATPase activity and microtubule-gliding function, without directly competing with ATP and microtubule binding. Molecular modeling of Eg5 and KLF interaction revealed a stable Eg5-KLF complex where the biflavonoid was suitably accommodated within the L5/α2/α3 allosteric pocket. The binding of KLF to the binding pocket reduced the solvation of both the allosteric and nucleotide-binding pockets and altered the conformation of Eg5. Our data suggest that KLF, from the medicinal plant *Garcinia*, is a novel allosteric inhibitor of mitotic kinesin Eg5.

Chapter 4

General discussion

&

Summary

General Discussions

The goal of this research is developing a novel kinesin Eg5 inhibitor with a photo-switching mechanism and regulate the activities of the mitotic kinesin Eg5 precisely. To achieve that, I demonstrated to develop an inhibitor which composed of two parts such as regulatory and inhibitory part. First, I emphasized on to establish a regulatory part utilizing photochromic inhibition. Subsequently, I discovered an Eg5 inhibitor from the natural sources.

To date, there are several effective Eg5 inhibitors that are well-known. Surprisingly, the inhibitors have the same binding pocket at the nucleotide binding site, which is made up of loop L5, helix 2, and helix 3, and the structure of the inhibitors are not well conserved. The aromatic rings connected by rotatable single bonds with localized polar functional groups are the unique structural feature shared by all typical potent Eg5 inhibitors.

The photochromic molecules, which are comparable to the inhibitors previously described, were thought to have a photo-reversible inhibitory action on Eg5. ACTAB, an STLC derivative comprised of photo-chromic azobenzene molecules, has already reported as an inhibitor with photo-reversible action. In the structure of ACTAB, the azobenzene is positioned between the trithyl group and the cysteine of STLC. The cis-trans photo-isomerization of ACTAB resulted in a variety of inhibitory actions. Following that, the photochromic chemical derivative was shown to function as an Eg5 inhibitor with a photo-switching mechanism.

In this study, spiropyran and azobenzene were used as photochromic molecules to synthesize Eg5 inhibitor SPSAB. When UV and VIS irradiated, spiropyran isomerizes into a hydrophobic closed ring SP-form and a zwitterionized open ring MC-form. However, azobenzene forms trans and cis isomer when it irradiated to Vis and UV light. Ispinesib, a potent Eg5 inhibitor, has a structure similarity to spiropyran.

There was a significant alteration in inhibitory action associated with its isomerization, which consisted of spiropyran and azobenzene, as a photochromic Eg5 inhibitor, which was highly anticipated. SPSAB inhibited the basal ATPase activity of Eg5 more effectively than another photochromic inhibitor, ACTAB, as noted previously.

The polarity of the solvent in the dark is used to convert the SP isomer of spiropyran to the MC isomer. The concentration of the MC isomer grows as the water content of the binary solvent combination increases in the thermal equilibrium condition. In an aqueous solution, SPSAB also demonstrated reverse photochromism. In the dark, the closed ring, colorless SP-form of SPSAB automatically changed to the open ring, colorful MC-form. The reverse photochromism was not seen in a plain or organic solvent. Since this rapid conversion of SP to MC of SPSAB in the dark was slower than under UV irradiation, SP-MC isomerization may be detected using VIS and darkness rather than UV light.

Finally, different inhibitory activity on Eg5 ATPase was observed among the three isomers of SPSAB. The degree of inhibition was varied in each photoisomerization, and the most obstructive inhibition was observed by SP-trans form. Surprisingly, there was a substantial variation in control across the three states. As a result, this work demonstrated that photochromic molecules may be used as a photo-switching device to regulate the inhibitory activity of the mitotic kinesin Eg5 inhibitor.

Subsequently, the inhibitory part of Eg5 inhibitor was derived from the natural compound which is Kolaflavanone (KLF) a *Garcinia* species. It has already been reported that the extract of Garcinia kola and the active compound of it is bioflavonoids are chemically and biologically active and showed therapeutic benefits, including anti-diabetic, anti-inflammatory, and anti-proliferative properties (*93,94*). Anticancer action has been observed in biflavonoids from a variety of plants, however the molecular targets and underlying mechanisms for this

effect are yet unknown (*54–56*). KLF has been found to inhibit tyrosinase (*60*), as interact with serum albumin and aldehyde dehydrogenase, an essential enzyme in detoxification processes (*61, 62*).

Additionally, KLF showed anti-proliferative and anti-angiogenic properties in vitro, as favorable benefits in the treatment of benign prostatic hyperplasia. Reports have shown that Kinesin Eg5 is overexpress in cancer cell and small molecules may inhibit the Kinesin Eg5 activity and induce monopolar spindle formation. Hence, KLF may be applicable as an inhibitor for Kinesin Eg5.

However, the biochemical study of KLF-Eg5 interactions has not done yet. As a result, I investigated the influence of KLF on Eg5 ATPase and motility activities. The findings provided in this work showed that KLF inhibits Eg5 ATPase and microtubule-gliding activities allosterically, as the probable mechanisms of Eg5–KLF interaction.

Summary

kinesin Eg5 is essential for the bipolar spindle formation in eukaryotic cell division. It is overexpressed in the cancer cell and considered a target for malignancy treatment. It has been reported that small chemical compounds control the activity of Eg5 and obstruct the formation of bipolar spindle formation and hence induce monopolar formation. In this study, I developed a novel functional inhibitor for mitotic kinesin Eg5 as a target cancer therapy. The functional inhibitor was designed by coupling the regulatory and inhibitory parts. The regulatory part was composed of photochromic compounds which control Eg5 activity in multiple state isomerization (SPSAB). On the other hand, I discovered a chemical compound from natural sources (Kolaflavanone) for the inhibitory part. Interestingly, the biochemical characterization and docking simulation results of Kolaflavanone demonstrated its inhibitory activity on Eg5. Therefore, the overall result suggests that the aim of the study has been completely fulfilled.
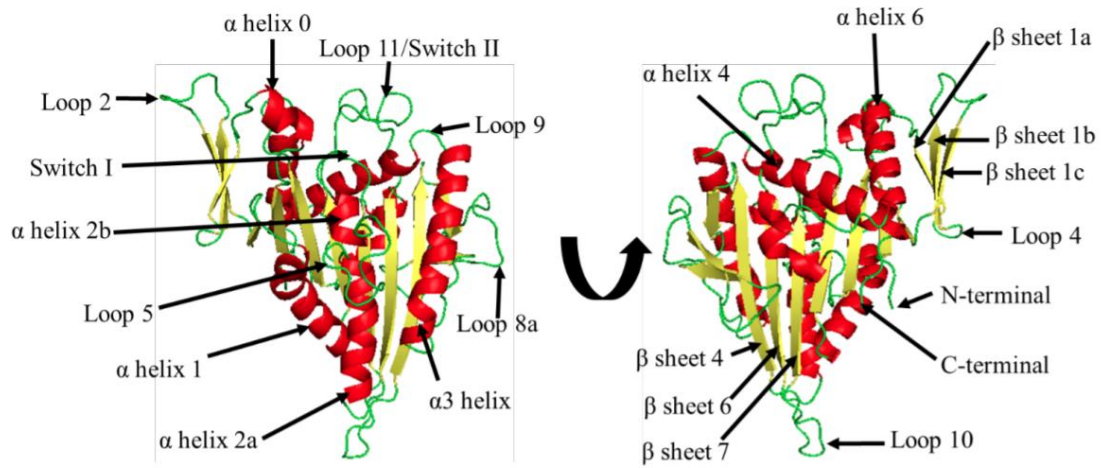
Supplementary Fig. 1

References

1. Hirokawa, N., & Noda, Y. (2008). Intracellular transport and kinesin superfamily proteins, KIFs: structure, function, and dynamics. *Physiological reviews*, *88*(3), 1089-1118.

2. Vale, R. D., Reese, T. S., & Sheetz, M. P. (1985). Identification of a novel force-generating protein, kinesin, involved in microtubule-based motility. *Cell*, *42*(1), 39-50.

3. Vale, R. D., & Fletterick, R. J. (1997). The design plan of kinesin motors. *Annual review of cell and developmental biology*, *13*(1), 745-777.

4. Rath, O., & Kozielski, F. (2012). Kinesins and cancer. *Nature reviews cancer*, *12*(8), 527-539.

5. Kull, F. J., Vale, R. D., & Fletterick, R. J. (1998). The case for a common ancestor: kinesin and myosin motor proteins and G proteins. *Journal of Muscle Research & Cell Motility*, *19*(8), 877-886.

6. Harrington, T. D., Naber, N., Larson, A. G., Cooke, R., Rice, S. E., & Pate, E. (2011). Analysis of the interaction of the Eg5 Loop5 with the nucleotide site. *Journal of theoretical biology*, *289*, 107-115.

7. Huszar, D., Theoclitou, M. E., Skolnik, J., & Herbst, R. (2009). Kinesin motor proteins as targets for cancer therapy. *Cancer and Metastasis Reviews*, *28*(1), 197-208.

8. Sarli, V., & Giannis, A. (2006). Inhibitors of mitotic kinesins: next generation antimitotics. *ChemMedChem: Chemistry Enabling Drug Discovery*, *1*(3), 293-298.

9. Ishikawa, K., Tohyama, K., Mitsuhashi, S., & Maruta, S. (2014). Photocontrol of the mitotic kinesin Eg5 using a novel S-trityl-l-cysteine analogue as a photochromic inhibitor. *The Journal of Biochemistry*, *155*(4), 257-263.

10. KOBATAKE, S., & IRIE, M. (2007). Reversible Shape Changes of Photochromic Molecular Crystals upon Photoirradiation. *Nihon Kessho Gakkaishi*, *49*(4), 238-243.

11. Ulaganathan, V., Talapatra, S. K., Rath, O., Pannifer, A., Hackney, D. D., and Kozielski, F. (2013) Structural insights into a unique inhibitor binding pocket in kinesin spindle protein. *J. Am. Chem. Soc.* 135(6), 2263-2272

12. Beer, T. M., Goldman, B., Synold, T. W., Ryan, C. W., Vasist, L. S., Van Veldhuizen Jr, Dakhil, S. R., Lara Jr, P. N., Drelichman, A., Hussain, M. H. A., Crawford, E. D. (2008) Southwest Oncology Group phase II study of ispinesib in androgen-independent prostate cancer previously treated with taxanes. *Clin. Genitourin. Cancer.* 6(2), 103-109

13. Verhey, K. J., and Hammond, J. W. (2009) Traffic control: regulation of kinesin motors. *Nat. Rev. Mol. Cell Biol.*. 10(11), 765-777

14. Rath, O., and Kozielski, F. (2012) Kinesins and cancer. *Nat. Rev. Cancer.* 12(8), 527

15. Kaan, H. Y. K., Major, J., Tkocz, K., Kozielski, F., and Rosenfeld, S. S. (2013) "Snapshots" of ispinesib-induced conformational changes in the mitotic kinesin Eg5. *J. Biol. Chem.* 288(25), 18588-18598

16. Ishikawa, K., Tamura, Y., and Maruta, S. (2014) Photocontrol of mitotic kinesin Eg5 facilitated by thiol-reactive photochromic molecules incorporated into the loop L5 functional loop. *J. Biochem.* 155(3), 195-206

17. García-Amorós, J., and Velasco, D. (2012) Recent advances towards azobenzene-based light-driven real-time information-transmitting materials. *Beilstein J. Org. Chem.* 8(1), 1003-1017

18. Rau, H. (1990) *Azo compounds in photochromism: Molecules and Systems* (Durr, H. and Bouas- Laurent, H., eds) pp. 165-192, Elsevier, Amsterdam

19. Ichimura, K., Seki, T., Kawanishi, Y., Suzuki, Y., Sakuragi, M., and Tamaki, T. (1996) Photocontrol of liquid crystal alignment by " command surface" in Photoreactive Materials for Ultrahigh Density Optical Memory (Irie, M., ed.) pp. 55-88, Elsevier, Amsterdam.

20. Irie, M., Fukaminato, T., Sasaki, T., Tamai, N., and Kawai, T. (2002) Organic chemistry: a digital fluorescent molecular photoswitch. Nature. 420 (6917), 759-760

21. Kimura, K., Mizutani, R., Suzuki, T., and Yokohama, M. (1998) Photochemical ionic conductivity switching systems of photochromic crown ethers for information technology. *J. Inclusion Phenom.* 32(2-3), 295-310

22. Klajn, R. (2014) Spiropyran-based dynamic materials. *Chem. Soc. Rev.* 43(1), 148-184

23. Ishikawa, K., Tohyama, K., Mitsuhashi, S., and Maruta, S. (2014) Photocontrol of the mitotic kinesin Eg5 using a novel S-trityl-l-cysteine analogue as a photochromic inhibitor. *J. Biochem.* 155(4), 257-263

24. Sadakane, K., Alrazi, I. M., and Maruta, S. (2018) Highly efficient photocontrol of mitotic kinesin Eg5 ATPase activity using a novel photochromic compound composed of two azobenzene derivatives. *J. Biochem.* 164(4), 295-301

25. Sadakane, K., Takaichi, M., and Maruta, S. (2018) Photo-control of the mitotic kinesin Eg5 using a novel photochromic inhibitor composed of a spiropyran derivative. *J. Biochem.* 164(3), 239-246

26. Kalisky, Y., Orlowski, T. E., and Williams, D. J. (1983) Dynamics of the spiropyran-merocyanine conversion in solution. *J. Phys. Chem.* 87(26), 5333-5338

27. Rau, H. (1990) *Photochemistry and photophysics* pp. 119-141, CRC, Boca Raton, FL

28. Sawin, K.E., LeGuellec, K., Philippe, M., and Mitchison, T.J. (1992). Mitotic spindle organization by a plus-end-directed microtubule motor. *Nature* **359**, 540–543.

29. Cole, D.G., Saxton, W.M., Sheehan, K.B., and Scholey, J.M. (1994) A "slow" homotetrameric kinesin-related motor protein purified from Drosophila embryos. *J. Biol Chem.* **269,** 22913–22916.

30. Kashina, A.S., Baskin, R.J., Cole, D.G., Idaman, K.P., Saxton, W.M., and Scholey, J.M. (1996a) A bipolar kinesin. *Nature* **379**, 270–272.

31. Kashina, A.S., Scholey, J.M., Leszyk, J.D., and Saxton, W.M. (1996b) An essential bipolar mitotic motor. *Nature* **384**:225.

32. Kapitein, L.C., Peterman, E.J., Kwok, B.H, Kim, J.H., Kapoor, T.M., and Schmidt, C.F. (2005) The bipolar mitotic kinesin Eg5 moves on both microtubules that it crosslinks. *Nature* **435**, 114–118.

33. Acar, S., Carlson, D.B., Budamagunta, M.S., Yarov-Yarovoy, V., Correia, J.J., Niñonuevo, M.R., Jia, W., Tao, L., Leary, J.A., Voss, J.C., Evans, J.E., and Scholey, J.M. (2013) The bipolar assembly domain of the mitotic motor Kinesin-5. *Nat. Commun.* **4,**1343.

34. Hotha, S., Yarrow, J.C., Yang, J.G., Garrett, S., Renduchintala, K.V., Mayer, T.U., and Kapoor, T.M., (2003) HR22C16: a potent small-molecule probe for the dynamics of cell division, Angew. *Chem. Int. Ed.* **42**, 2379–2382.

35. Masuda, A., Maeno, K., Nakagawa, T., Saito, H., and Takahashi, T. (2003) Association betIen mitotic spindle checkpoint impairment and susceptibility to the induction of apoptosis by anti-microtubule agents in human lung cancers. *Am. J. Pathol.* **163**, 1109–1116.

36. DeBonis, S., Skoufias, D.A., Lebeau, L., Lopez, R., Robin, G., Margolis, R.L., Wade, R.H., and Kozielski, F. (2004) *In vitro* screening for inhibitors of the human mitotic kinesin Eg5 with antimitotic and antitumor activities. *Mol. Cancer Ther.* **3**, 1079–1090.

37. Sarli, V., and Giannis, A. (2006) Inhibitors of mitotic kinesins: next generation antimitotics. *ChemMedChem* **1**, 293–298.

38. Tang, Y., Orth, J.D., Xie, T., and Mitchison, T.J. (2011) Rapid induction of apoptosis during kinesin-5 inhibitor-induced mitosis arrest in HL60 cells. *Cancer Lett.* **310**, 15–24.

39. Jiang, C., Yang, L., Wu, W., Guo, Q., and You, Q. (2011) CPUYJ039, a newly synthesized benzimidazole-based compound, is proved to be a novel inducer of apoptosis in HCT116 cells with potent KSP inhibitory activity. *J. Pharm. Pharmacol.* **63**, 1462–1469.

40. Sakowicz, R., Finer, J.T., Beraud, C., Crompton, A., Lewis, E., Fritsch, A., Lee, Y., Mak, J., Moody, R., Turincio, R., Chabala, J.C., Gonzales, P., Roth, S., Iitman, S., and Wood, K.W. (2004) Antitumor activity of a kinesin inhibitor. *Cancer Res.* **64,** 3276–3280.

41. Jackson, J.R., Patrick, D.R., Dar, M.M., and Huang, P.S. (2007) Targeted anti-mitotic therapies: can I improve on tubulin agents? *Nat. Rev. Cancer* **7**, 107–117.

42. Lad, L., Luo, L., Carson, J.D., Wood, K.W., Hartman, J.J., Copeland, R.A., and Sakowicz, R. (2008) Mechanism of inhibition of human KSP by ispinesib. *Biochemistry* **47**, 3576–3585.

43. Cochran, J.C., Gatial, J.E. 3rd, Kapoor, T.M., and Gilbert, S.P. (2005) Monastrol inhibition of the mitotic kinesin Eg5. *J. Biol. Chem.* **280**, 12658–12667.

44. DeBonis, S., Skoufias, D.A., Lebeau, L., Lopez, R., Robin, G., Margolis, R.L., Wade, R.H., and Kozielski, F. (2004) *In vitro* screening for inhibitors of the human mitotic kinesin Eg5 with antimitotic and antitumor activities. *Mol. Cancer Ther.* **3**, 1079–1090.

45. Nakazawa, J., Yajima, J., Usui, T., Ueki, M., Takatsuki, A., Imoto, M., Toyoshima, Y.Y., and Osada, H. (2003) A novel action of terpendole E on the motor activity of mitotic kinesin Eg5. *Chem. Biol.* **10**, 131–137.

46. Reddie, K.G., Roberts, D.R., and Dore, T.M. (2006) Inhibition of kinesin motor proteins by adociasulfate-2. *J. Med. Chem.* **49,** 4857–4860.

47. Iwu, M. (1985) Antihepatoxic constituents of Garcinia kola seeds. *Experientia* **41**, 699–700.

48. Iwu, M.M., Igboko, O.A., Onwuchekwa, U., and Okunji, C.O. (1987) Evaluation of the anti-hepatotoxicity of the biflavonoids of Garcinia kola seeds. *J. Ethnopharmacol.* **21**, 127–142.

49. Iwu, M.M., Igboko, O.A., Okunji, C.O., and Tempesta, M.S. (1990) Antidiabetic and aldose reductase activities of biflavanones of *Garcinia kola*. *J. Pharm. Pharmacol.* **42**, 290–292.

50. Adaramoye, O.A., Nwaneri, V.O., Anyanwu, K.C., Farombi, E.O., and Emerole, G.O. (2005) Possible anti-atherogenic effect of Kolaviron (a Garcinia kola seed extract) in hypercholesterolaemic rats. *Clin. Exp. Pharmacol. Physiol*. **32**, 40–46.

51. Braide, V.B. (1993) Anti-inflammatory effect of Kolaviron, bio-flavonoid extract of Garcinia kola. *Fitoterapia* **64**, 433–436.

52. Farombi, E.O., Adedara, I.A., Ajayi, B.O., Ayepola, O.R., and Egbeme, E.E. (2013) Kolaviron, a natural antioxidant and anti-inflammatory phytochemical prevents dextran sulphate sodium-induced colitis in rats. *Basic Clin. Pharmacol. Toxicol.* **113**, 49–55.

53. Igado, O.O., Olopade, J.O., Adesida, A., Aina, O.O., and Farombi, E.O. (2012) Morphological and biochemical investigation into the possible neuroprotective effects of kolaviron (*Garcinia kola* bioflavonoid) on the brains of rats exposed to vanadium. *Drug Chem. Toxicol*. **35**, 371–380.

54. Thapa, A., Woo, E.R., Chi, E.Y., Sharoar, M.G., Jin, H., Shin, S.Y., and Park, I. (2011) Biflavonoids are superior to monoflavonoids in inhibiting amyloid-β toxicity and fibrillogenesis via accumulation of nontoxic oligomer-like structures. *Biochemistry*. **50**, 2445–2455.

55. Daniel, J.F., Alves, C.C., Grivicich, I., da Rocha, A.B., and de Carvalho, M.G. (2007) Antitumor activity of biflavonoids from Ouratea and Luxemburgia on human cancer cell lines. *Indian J. Pharmacol.* **39**, 184–186.

56. Pang, X., Yi, T., Yi, Z., Cho, S.G., Qu, W., Pinkaew, D., Fujise, K., and Liu, M. (2009) Morelloflavone, a biflavonoid, inhibits tumor angiogenesis by targeting rho GTPases and extracellular signal-regulated kinase signaling pathways. *Cancer Res.* **69**, 518–525.

57. Mostafa, N.M., Ashour, M.L., Eldahshan, O.A., and Singab, A.N. (2015) Cytotoxic activity and molecular docking of a novel biflavonoid isolated from *Jacaranda acutifolia* (Bignoniaceae). *Nat. Prod. Res.* **23**, 1–8.

58. Kalu, W.O., Okafor, P.N., Ijeh, I.I. and Eleazu, C. (2016) Effect of kolaviron, a biflavanoid complex from Garcinia kola on some biochemical parameters in experimentally induced benign prostatic hyperplasic rats. *Biomed. Pharmacother.* **83**:1436–1443.

59. Muhammad, A., Funmilola, A., Aimola, I.A., Ndams, I.S., Inuwa, M.H., and Nok, A.J. (2017) Kolaviron shows anti-proliferative effect and down regulation of vascular endothelial growth factor-C and toll like receptor-2 in *Wuchereria bancrofti* infected blood lymphocytes. *J. Infect. Public Health.* **10**, 661–666.

60. Ogunwa, T.H., Taii, K., Sadakane, K., Kawata, Y., Maruta, S., and Miyanishi, T. (2019A) Morelloflavone as a novel inhibitor of mitotic kinesin Eg5. *J. Biochem.* **166**, 129–137.

61. Okunji, C., Komarnytsky, S., Fear, G., Poulev, A., Ribnicky, D.M., Awachie, P.I., Ito, Y., and Raskin, I. (2007) Preparative isolation and identification of tyrosinase inhibitors from the seeds of *Garcinia kola* by high-speed counter-current chromatography. *J. Chromatography A.* **1151**, 45–50.

62. Kolawole, A.N., Akinladejo, V., Elekofehinti, O.O., Akinmoladun, A.C., and Kolawole, A.O. (2018) Experimental and computational modeling of interaction of kolaviron-kolaflavanone with aldehyde dehydrogenase. *Bioorg. Chem.* **78**, 68–79.

63. Kolawole, A.O., Kolawole, A.N., Olofinsan, K.A., and Elekofehinti, O.O. (2020) Kolaflavanone of kolaviron selectively binds to subdomain 1B of human serum albumin: spectroscopic and molecular docking evidence. *Comp. Toxicol.* **13**, 100118.

64. Sadakane, K., Alrazi, I. M., & Maruta, S. (2018). Highly efficient photocontrol of mitotic kinesin Eg5 ATPase activity using a novel photochromic compound composed of two azobenzene derivatives. The Journal of Biochemistry, 164, 295-301.

65. Hackney, D.D. (1988) Kinesin ATPase: rate-limiting ADP release. *Proc. Natl. Acad. Sci.* USA. **85**, 6314–6318.

66. Youngburg, G.E. and Youngburg, M.V. (1930) Phosphorus metabolism. I. A system of blood phosphorus analysis. *J. Lab. Clin. Med.* **16**, 158–166.

67. Alrazi, I., Sadakane, K., & Maruta, S. (2021). Novel photochromic inhibitor for mitotic kinesin Eg5 which forms multiple isomerization states. *J. Biochem.* **in press.** https://doi.org/10.1093/jb/mvab035

68. Seeliger, D. and de Groot, B.L. (2010) Ligand docking and binding site analysis with PyMol and Autodock/Vina. *J. Comput. Aided Mol. Des.* **24**, 417–422.

69. Trott, O. and Olson, A.J. (2010) AutoDock Vina: Improving the speed and accuracy of docking with a new scoring function, efficient optimization and multithreading. *J. Comput. Chem.* **31**, 455–461.

70. Van Der Spoel, D., Lindahl, E., Hess, B., Groenhof, G., Mark, A. E., and Berendsen, H. J. (2005) GROMACS: Fast, flexible, and free. *J. Comput. Chem.* 26, 1701–1718.

71. Hornak V, Abel R, Okur A, Strockbine B, Roitberg A, and Simmerling C (2006) Comparison of multiple Amber force fields and development of improved protein backbone parameters. *Proteins Struct. Funct. Bioinf.* **65**, 712–725.

72. Hess, B., Bekker, H., Berendsen, H. J. C., and Fraaije, J. G. E. M. (1997) LINCS: A linear constraint solver for molecular +simulations. *J. Comput. Chem.* **18**, 1463–1472.

73. Nagarajan, S. and Sakkiah, S. (2018) Exploring a potential allosteric inhibition mechanism in the motor domain of human Eg5. *J. Biomol. Struct. Dyn.* **13**, 1–27.

74. Maliga, Z., Kapoor, T.M., and Mitchison, T.J. (2002) Evidence that monastrol is an allosteric inhibitor of the mitotic kinesin Eg5. *Chem. Biol.* **9**, 989–996

75. Lad, L., Luo, L., Carson, J.D., Wood, K.W., Hartman, J.J., Copeland, R.A., and Sakowicz, R. (2008) Mechanism of inhibition of human KSP by ispinesib. *Biochemistry* **47**, 3576–3585.

76. Wang, F., Good, J.A., Rath, O., Kaan, H.Y., Sutcliffe, O.B., Mackay, S.P., and Kozielski, F. (2012) Triphenylbutanamines: kinesin spindle protein inhibitors with in vivo antitumor activity. *J. Med. Chem.* **55**, 1511–1525.

77. Cochran, J.C., Sontag, C.A., Maliga, Z., Kapoor, T.M., Correia, J.J., and Gilbert, S.P. (2004) Mechanistic analysis of the mitotic kinesin Eg5. *J. Biol. Chem.* **279**, 38861–38870.

78. Waldrop, G. L. (2009) A qualitative approach to enzyme inhibition. *J. Chem. Educ.* **37**, 11–15.

79. Turner, J., Anderson, R., Guo, J., Beraud, C., Fletterick, R., and Sakowicz, R. (2001) Crystal structure of the mitotic spindle kinesin Eg5 reveals a novel conformation of the neck-linker. *J. Biol. Chem.* **276**, 25496–25502.

80. Moores, C.A. (2010) Kinesin-5 mitotic motors: Is loop5 the on/off switch? *Cell Cycle* **9**, 1286–1290.

81. Harrington, T.D., Naber, N., Larson, A.G., Cooke, R., Rice, S.E., and Pate, E. (2011) Analysis of the interaction of the Eg5 Loop5 with the nucleotide site. *J. Theor. Biol.* **289**, 107–115.

82. Ogunwa, T.H., Laudadio, E., Galeazzi, R., and Miyanishi, T. (2019B) Insights into the molecular mechanisms of Eg5 inhibition by morelloflavone. *Pharmaceuticals* (Basel), **12**, 58.

83. Tcherniuk, S., van Lis, R., Kozielski, F., and Skoufias, D.A. (2010) Mutations in the human kinesin Eg5 that confer resistance to monastrol and S-Trityl-L-Cysteine in tumor derived cell lines. *Biochem. Pharmacol.* **79,** 864.

84. Jiang, C., Chen, Y., Wang, X., and You, Q. (2007) Docking studies on kinesin spindle protein inhibitors: an important cooperative 'minor binding pocket' which increases the binding affinity significantly. *J. Mol. Model.* **13**, 987–992.

85. Kaan, H.Y.K., Ulaganathan, V., Hackney, D.D., and Kozielski, F. (2010) An allosteric transition trapped in an intermediate state of a new kinesin-inhibitor complex. *Biochem. J.* **425**, 55－60.

86. Talapatra, S.K., Schüttelkopf, A., and Kozielski, F. (2012) Crystal structure of the ternary Eg5-ADP-ispinesib complex. *Acta Cryst. D.* **68**, 1311–1319.

87. Yokoyama, H., Sawada, J.I., Sato, K., Ogo, N., Kamei, N., Ishikawa, Y., Hara, K., Asai, A., and Hashimoto, H. (2018) Structural and thermodynamic basis of the enhanced interaction betIen kinesin spindle protein Eg5 and STLC-type inhibitors. *ACS Omega.* **3**, 12284–12294.

88. Locke, J., Joseph, A.P., Pena, A., Mockel, M.M, Mayer, T.U., Topf, M, and Moores C.A. (2017) Structural basis of human kinesin-8 function and inhibition. PNAS, doi/10.1073/pnas.1712169114.

89. Shima, T., Morikawa, M., Kaneshiro, J., Kambara, T., Kamimura, S., Yagi, T., Iwamoto, H., Uemura, S., Shigematsu, H., Shirouzu, M., et al. (2018) Kinesin-binding-triggered conformation switching of microtubules contributes to polarized transport. *J. Cell Biol.* **217**, 4164–4183.

90. Gigant, B., Wang, W., Dreier, B., Jiang, Q., Pecqueur, L., Plückthun, A., Wang, C., and Knossow, M. (2013) Structure of a kinesin-tubulin complex and implications for kinesin motility. *Nat. Struct. Mol. Biol.* **20**, 1001–1007.

91. Chen, G., Cleary J.M., Asenjo, A.B., Chen, Y., Mascaro, J.A., Arginteanu, D.F.J., Sosa, H., and Hancock, W.O. (2019) Kinesin-5 promotes microtubule nucleation and assembly by stabilizing a lattice-competent conformation of tubulin. *Current Biol.* **29**, 2259–2269.

92. Scarabelli, G. and Grant, B.J. (2014) Kinesin-5 allosteric inhibitors uncouple the dynamics of nucleotide, microtubule, and neck-linker binding sites. *Biophys. J.* **107**, 2204–2213.

93. . Farombi, E. O., & Owoeye, O. (2011). Antioxidative and chemopreventive properties of Vernonia amygdalina and Garcinia biflavonoid. *International journal of environmental research and public health*, *8*(6), 2533-2555.

94. Ayepola, O. R., Brooks, N. L., & Oguntibeju, O. O. (2014). Kolaviron improved resistance to oxidative stress and inflammation in the blood (erythrocyte, serum, and plasma) of streptozotocin-induced diabetic rats. *The Scientific World Journal*, *2014*.